ABSTRACT

Title of dissertation: THE EFFECTS OF COUPLING DELAY AND AMPLITUDE / PHASE INTERACTION ON LARGE COUPLED OSCILLATOR NETWORKS

Wai Shing Lee, Doctor of Philosophy, 2013

Dissertation directed by: Professor Edward Ott
Department of Electrical and Computer Engineering
Professor Thomas M. Antonsen Jr.
Department of Electrical and Computer Engineering

The interaction of many coupled dynamical units is a theme across many scientific disciplines. A useful framework for beginning to understanding such phenomena is the coupled oscillator network description. In this dissertation, we study a few problems related to this.

The first part of the dissertation studies generic effects of heterogeneous interaction delays on the dynamics of large systems of coupled oscillators. Here, we modify the Kuramoto model (phase oscillator model) to incorporate a distribution of interaction delays. Corresponding to the continuum limit, we focus on the reduced dynamics on an invariant manifold of the original system, and derive governing equations for the system, which we use to study stability of the incoherent state and the dynamical transitional behavior from stable incoherent states to stable coherent states. We find that spread in the distribution function of delays can greatly alter

the system dynamics.

The second part of this dissertation is a sequel to the first part. Here, we consider systems of many spatially distributed phase oscillators that interact with their neighbors, and each oscillator can have a different natural frequency, and a different response time to the signals it receives from other oscillators in its neighborhood. By first reducing the microscopic dynamics to a macroscopic partial-differential-equation description, we then numerically find that finite oscillator response time leads to many interesting spatio-temporal dynamical behaviors, and we study interactions and evolutionary behaviors of these spatio-temporal patterns.

The last part of this dissertation addresses the behavior of large systems of heterogeneous, globally coupled oscillators each of which is described by the generic Landau-Stuart equation, which incorporates both phase and amplitude dynamics. Our first goal is to investigate the effect of a spread in the amplitude growth parameter of the oscillators and that of a homogeneous nonlinear frequency shift. Both of these effects are of potential relevance to recently reported experiments. Our second goal is to gain further understanding of the observation that, at large coupling strength, a simple constant-amplitude sinusoidal oscillation is always a solution for the dynamics of the global order parameter when the system has constant nonlinear characteristics.

THE EFFECTS OF COUPLING DELAY AND AMPLITUDE / PHASE INTERACTION ON LARGE COUPLED OSCILLATOR NETWORKS

by

Wai Shing Lee

Dissertation submitted to the Faculty of the Graduate School of the
University of Maryland, College Park in partial fulfillment
of the requirements for the degree of
Doctor of Philosophy
2013

Advisory Committee:
Professor Edward Ott, Chair
Professor Thomas M. Antonsen Jr.
Professor Michelle Girvan
Professor P. S. Krishnaprasad
Professor Rajarshi Roy (Dean's Representative)

Acknowledgements

Pursuit of a Ph.D. is an important step toward realization of my aspiration. I am very glad at this stage when completing this dissertation. When I look back through these years of study and research, there are indeed too many things that have supported me through. Without them, it would never be possible that I can find it an enjoyable moment when completing this dissertation now, which signifies to me a satisfactory completion to this stage of life.

First of all, I would like to express my deep gratitude to all my family members. Thanks to my parents who have always placed emphasis and allowed opportunities for their children to receive education. Thanks to my brother and sisters who have sustained the family. They have provided me an environment free of worry, which has allowed me the freedom to seek for my aspiration through all these years. Also, for their practical advices and urges that have always helped me fix my sight on the practical side of life while walking on this path of pursuit. Finally, thanks to the little kids at home too, they have indeed added much fun to the family.

The most important element of a dissertation is the academic content. In this regard, I would like to express my deep gratitude to my two advisors. Thanks for their inception of interesting problems, brave attempts to tackling problems, and the insightful ideas that truly get problems solved. From them I see how a piece of research work can be like construction of a building that has both style and

functional usage. It is very important that a good piece of research should contain both elements! Further, I would like to thank Prof. Ott for his many other major participations in my work like editing my papers and this dissertation, financial support during my research years, many precious opportunities allotted to me, and many other practical advices and helps throughout these years.

Lastly, I would like to thank the people of the nonlinear dynamics group at UMD, many friends of the Hong Kong student group, Episcopal / Anglican Campus Ministry, TaiChi group, and many other individual friends. All the togetherness we have had, discussions, and casual chats on work, fun and life, in private or on the internet, etc. These are all integral parts of my years of Ph.D. study, which I will treasure in my heart, and bring forward to the future challenges that I am heading into!

Table of Contents

List of Figures

Chapter 1

Introduction

1.1 Synchronization

Synchronization is a fundamental phenomena exhibited in many natural and engineered systems. The first recorded scientific description of synchronization was due to Huygens who reported that two pendulums suspended on the same wooden beam tended to move together. He further noticed that this tendency reestablished itself after it was disturbed. Thus it was a genuine effect intrinsic to the combined pendulums-beam system. Since then many other co-operative phenomena associated with the coupling of similar systems have been found. We now outline some examples.

In the mid-nineteenth century, Lord Rayleigh described in his book, *The theory of Sound*, a case where two organ pipes of the same pitch were situated next to each other, and, through their interaction, instead of making them sound at the same pitch, both were suppressed to silence. Synchronization also arises between very different systems. In the early twentieth century, Appleton and Van der Pol

found that the frequency of a triode generator could synchronize with another weak signal from a different source which was of slightly different frequency. Here, rather than two similar systems compromising on a common behavior, one of the systems simply follows that of the other. Furthermore, Synchronization is observed in living organisms as well. For instance, the daily 24-hour sleep/wake cycle of many animals is found to be governed by the circadian clock of the body, which is entrained to the 24-hour day-night period of the Earth. The operation of the circadian clock has been traced to functioning of the suprachiasmatic nucleus inside the brain. Two popular accounts dealing with physiological clocks can be found in Refs. [63, 59]. Other examples of physiological Synchronization occur for the heart and the intestine. In these cases, a remarkable aspect of Synchronization is that they involve not just a few interacting entities, but many such entities, e.g., the large number of pacemaker cells in the heart. Thus, Synchronization can be a truly *global* and *macroscopic* effect built on top of *local* and *microscopic* behaviors. Synchronization can also occur among physically well separated entities, which communicate by some means. For example, when certain species of fireflies gather on a tree, they can synchronize and flash in unison; in a similar vein, audience members in a concert hall can rather quickly synchronize their applause. These diverse examples show that Synchronization is a very general phenomenon spanning a broad variety of situations, including physical, biological, and even social situations; and crossing scales from the microscopic to the macroscopic.

1.2 Why coupled oscillator networks

In the previous section, we have seen some examples of Synchronization in vastly differing contexts. Despite differing details, a common theme underlying many of such situations is the building up of a *global macroscopic* response from *local microscopic* dynamics and interactions. In the spirit of reductionism, we assume that all complexities in the real world ultimately reduce to the functioning of its constituents. Therefore, e.g., in order to understand the human body, we move down level by level, first to functions of individual organs, like beating of the heart, then one level further down to functions of more microscopic constituents, like beating of the individual heart pacemaker cells. Then in order to study the higher level functioning of the heart as a whole, we move up the reductionist hierarchy again and suppose that each pacemaker cell has to interact with, or couple to, some other pacemaker cells, and we believe that it is through such coupling that the global synchronized beating of the heart arises. Indeed, nature has shown us that the final behavior of the heart beat has to be a coherent whole. Loss of such synchrony in the heart leads to serious pathologies.

One of the simplest ways to cast the above picture into simple mathematical models is to imagine each local entity, e.g., a single pacemaker cell, as a generic oscillator (the precise mathematical form to be specified with the precise questions under study), and then imagine a lot of such oscillators to interact with one another through some form of coupling. Through the study of such oscillator network models, we may hope to gain important insights into how, e.g, individual heart

pacemaker cells differing from one another, nevertheless beat collectively to make the heart beat as a coherent whole. Two important insights obtained from such modelings are that collective macroscopic behaviors of this sort depend crucially on how the local constituents are coupled together, and that the resulting system can exhibit a wide variety of behaviors when the coupling conditions change. Generally, for models of such coupled oscillator networks, three factors determine the overall dynamics of the system as a whole:

1. Dynamics of the individual isolated oscillators.

2. The topology according to which the oscillators are connected together.

3. The coupling dynamics through which each oscillator is coupled to other oscillators connected to it.

In this dissertation, motivated by physical considerations and recent experiments, we study, both theoretically and computationally, the properties of collective macroscopic behaviors of many coupled oscillators. In particular, we are concerned with large networks of coupled oscillators, i.e., networks comprising a very large number of oscillators, and we desire to consider a setting in which the individual oscillators are of sufficiently different character, mimicking what is normally the case with many real-world systems.

1.3 Methodology and layout of this dissertation

The primary focus of this dissertation is on the generic dynamical behavior of oscillator networks. As done previously by others, we assume very simple models

for the dynamics of oscillators. We note that despite our simple model dynamics, previous studies indicate that useful insights can be expected to result [57]. Noted examples include synchronous flashing of fireflies [8], pedestrian induced oscillations of the Millennium Bridge [65, 15, 1], cardiac pace-maker cells [19, 39], alpha rhythms in the brain [17], glycolytic oscillations in yeast populations [18, 13, 41], cellular clocks governing circadian rhythm in mammals [72], oscillatory chemical reactions [24, 67], coupled lasers [25, 70, 73], Josephson junction circuits [36, 50], etc. While real-world oscillators and their interaction networks can be complicated, the simplifications that we will employ make the problems tractable and enable discovery of generic collective phenomena and mechanisms that may be insensitive to the detailed behavior of individual oscillators. One useful model that has received wide attention is the Kuramoto Model [26, 27]. For this model, the fundamental microscopic dynamics of individual oscillators are assumed to be stable limit-cycle oscillations. This model further assumes that coupling among oscillators is "weak" enough that the limit cycle amplitude is very stable. Then the effects from all other oscillators on any other oscillator affect only the phase on its limit cycle. The first two problems studied in this dissertation involve large coupled oscillator networks of the Kuramoto type. In particular, the question that motivates us, is the effects of time delay due to, for example, finite signal propagation speed or finite response time. In Chapter 2 we study the problem in the context of an all-to-all coupled population of phase oscillators, and contrast the resulting behavior with the classical model without time delay, and with models with treatments of time delays but in a more restricted form. We show that many interesting dynamical behaviors

result from time delay. Then in Chapter 3, we further extend this consideration by imagining the oscillators to be distributed in space, and to interact with other oscillators in their neighborhood. We see that time delay in this spatial setting induces a variety of interesting spatio-temporal behavior. Then in Chapter 4 we study a problem related to oscillator networks made up of oscillators which allow more dynamics than that of the Kuramoto type. Recall that the phase oscillator model is useful when the interaction among oscillators is weak; therefore, it may no longer be adequate when the interaction is strong. In such cases we need to account for temporal evolution of both the oscillators' amplitudes as well as their phases. In order to understand systems with this type of dynamics, we employ the Landau-Stuart oscillator model [57], and consider the network dynamics that results upon coupling many such Landau-Stuart oscillators. On the experimental front, a motivation for considering this class of oscillator networks is due to recent experiments [67] which show results that cannot be described using the phase-only oscillator dynamics approach of the Kuramoto Model.

Chapter 2

Dynamics of large coupled oscillator networks with time-delayed interactions

2.1 Introduction

As introduced in Chapter 1, studies of large networks of coupled oscillators have been motivated by diverse real examples and considerations. However, an incompletely understood aspect of such problems is that signal propagation may take non-negligible time, and that systems often have a finite reaction time to inputs that they receive. Time delays are thus both natural and inevitable in many of these systems. In order to elucidate phenomena induced by time delay in large coupled oscillator systems, Refs. [69, 10] and [23, 43] carried out studies of globally coupled oscillators of the Kuramoto type ([26], [27]) in the presence of time delay. These previous works all treated the special case in which all time delays between interacting oscillators were identical, and, in that context, they uncovered many interesting behaviors revealing that time delay can profoundly affect the dynamics

of coupled oscillator systems. However, in most situations where delays are an important consideration, the delays are not all identical. The aim of this chapter is to study the more realistic case where there is a distribution of time delays along the links connecting the oscillators. We shall see that previous striking features obtained in the case of uniform time delay are evidently strongly dependent on coherent communication between oscillators, and, as a consequence, are substantially changed by the incorporation of even modest spread in the time delays. For example, comparing results for typical cases with uniform delay and with a 30% spread in delay, we will show that this delay spread (a) can completely eliminate the resonant structure in the average delay time dependence of the critical coupling k_c for the onset of coherence, (b) can introduce hysteresis into the system behavior, and (c) can substantially decrease the number of attractors that simultaneously exist in a given situation.

2.2 Formulation

We consider a network of oscillators with all-to-all coupling according to the classical Kuramoto scheme, but incorporating link-dependent interaction time delays τ_{ij} for coupling between any two oscillators i and j,

$$\frac{d}{dt}\theta_i(t) = \omega_i + (k/N)\sum_{j=1}^{N}\sin\left[\theta_j(t-\tau_{ij}) - \theta_i(t)\right], \tag{2.1}$$

where $\theta_i(t)$ is the phase of oscillator i, ω_i is the natural frequency of oscillator i, k characterizes the coupling strength between oscillators, N is the total number of oscillators, $\tau_{ii} = 0$, and $i = 1, 2 \cdots N$. Following Kuramoto, we note that the effect

of all the oscillators in the network on oscillator i may be expressed in terms of an "order parameter" r_i,

$$N^{-1}\sum_{j=1}^{N}\sin(\theta_j(t-\tau_{ij})-\theta_i(t)) = \mathrm{Im}[r_i e^{-i\theta_i(t)}], \tag{2.2}$$

$$r_i(t) = N^{-1}\sum_{j=1}^{N} e^{i\theta_j(t-\tau_{ij})}. \tag{2.3}$$

To facilitate the analysis, we consider the following two simplifying assumptions. First, we consider the continuum limit $N \to \infty$ appropriate to the study of large systems, $N \gg 1$. Second, we assume the collection of all delays τ_{ij} is characterized by a distribution $h(\tau)$ such that the fraction of links with delays between τ and $\tau+d\tau$ is $h(\tau)d\tau$. We, furthermore, assume that, for randomly chosen links, τ is uncorrelated with the oscillator frequencies ω at either end of the link. These assumptions enable a description of the system dynamics in terms of a single oscillator distribution function $f(\theta,\omega,t)$, which evolves in response to a mean field $r(t)$ according to the following oscillator continuity equation,

$$\frac{\partial}{\partial t}f + \frac{\partial}{\partial\theta}\left\{\left[\omega + \frac{k}{2i}\left(e^{-i\theta}r - e^{i\theta}r^*\right)\right]f\right\} = 0. \tag{2.4}$$

In this case, the mean field $r(t)$ is given by

$$r(t) = \int_0^\infty \xi(t-\tau)h(\tau)d\tau, \tag{2.5}$$

$$\xi(t) = \int_{-\infty}^{\infty}\int_0^{2\pi} f(\omega,\theta,t)e^{i\theta}d\theta d\omega, \tag{2.6}$$

where Eq. (2.6) gives the input that nodes would receive in the absence of delay,

and Eq. (2.5) "corrects" this input by incorporating the appropriate delay for each fraction of inputing links, $h(\tau)d\tau$, with delay τ.

Expanding $f(\omega, \theta, t)$ in a Fourier series, we have

$$f(\omega, \theta, t) = \frac{g(\omega)}{2\pi}\left\{1 + \sum_{n=1}^{\infty}\left[f_n(\omega, t)e^{in\theta} + f_n^*(\omega, t)e^{-in\theta}\right]\right\}$$

where $g(\omega) \equiv \int_0^{2\pi} f(\omega, \theta, t)d\theta$ is the time-independent oscillator frequency distribution. Following the method outlined in [53], we consider the dynamics of Eq. (2.4) on an invariant manifold in f-space:

$$f_n(\omega, t) = [a(\omega, t)]^n. \tag{2.7}$$

The macroscopic dynamics of $a(\omega, t)$ can be derived by substituting Eq. (2.7) into Eq. (2.4), leading to

$$\partial a/\partial t + i\omega a + (k/2)\left(ra^2 - r^*\right) = 0. \tag{2.8}$$

In the case when the oscillator frequency distribution $g(\omega)$ is Lorentzian, i.e.,

$$g(\omega) = \frac{\Delta/\pi}{(\omega - \omega_0)^2 + \Delta^2}, \tag{2.9}$$

and assuming suitable properties of the analytic continuation into complex ω of $a(\omega, t)$ (see Ref. [53]), Eq. (2.6) can be evaluated explicitly by contour integration with the contour closing at infinity in the lower half complex ω-plane to give $\xi(t) = \int_{-\infty}^{\infty} g(\omega)a^*(\omega, t)d\omega = a^*(\omega_0 - i\Delta, t)$. Thus Eq. (2.5) becomes

$$r(t) = \int_0^{\infty} a^*(t - \tau)h(\tau)d\tau. \tag{2.10}$$

Furthermore, by setting $\omega = \omega_0 - i\Delta$ in Eq. (2.8) we have

$$\frac{d}{dt}a(t) + (\Delta + i\omega_0)a(t) + \frac{k}{2}\left(r(t)a(t)^2 - r^*(t)\right) = 0, \tag{2.11}$$

where in both Eqs. (2.10) and (2.11) the particular argument value $\omega = \omega_0 - i\Delta$ has been suppressed; i.e., $a(\omega_0 - i\Delta, t)$ is replaced by $a(t)$. Equations (2.10) and (2.11) thus form a complete description for the dynamics on the invariant manifold (2.7) when $g(\omega)$ is Lorentzian. Recently a result has been obtained [54] that, when applied to our problem, establishes that all attractors of the full system, Eqs. (2.4) - (2.6), are also attractors of our reduced system, Eqs. (2.10) and (2.11), and vice versa. (The result of Ref. [54] was previously strongly indicated by numerical experiments of Ref. [34].)

Previous studies of the effect of delay on the Kuramoto system (Refs. [69, 10, 23, 43]) considered uniform delay on all the links, corresponding to $h(\tau) = \delta(\tau - T)$. Our goal is to uncover the effect of heterogeneity of delays along the network links. Accordingly, we consider that $h(\tau)$ has some average value T with a spread about this value, and $h(\tau) \equiv 0$ for $\tau < 0$. A convenient class of functions for this purpose is

$$h(\tau) = \frac{1}{T}\hat{h}_n\left(\frac{\tau}{T}\right), \text{where } \hat{h}_n(\hat{\tau}) = A_n \hat{\tau}^n e^{-\beta_n \hat{\tau}}. \tag{2.12}$$

Here, A_n and β_n are determined by the normalization conditions: $\int_0^\infty \hat{h}_n(\hat{\tau})d\hat{\tau} = 1$ and $\int_0^\infty \hat{\tau}\hat{h}_n(\hat{\tau})d\hat{\tau} = 1$, yielding

$$A_n = (n+1)^{n+1}/n! \ , \ \ \beta_n = n+1. \tag{2.13}$$

For this family of distributions, we have that the standard deviation of τ about its mean T is given by

$$\delta\tau = (<\tau^2> - <\tau>^2)^{1/2} = T/\sqrt{n+1}. \tag{2.14}$$

Thus, for $n \to \infty$, we recover the case, $h(\tau) = \delta(\tau - T)$, previously investigated in Refs. [69, 10, 23, 43]. And, by decreasing n, we can study the effect of increasing the relative spread $\delta\tau/T$ in the delay times. The dependence of $h(\tau)$ on n is depicted in Fig. 2.1.

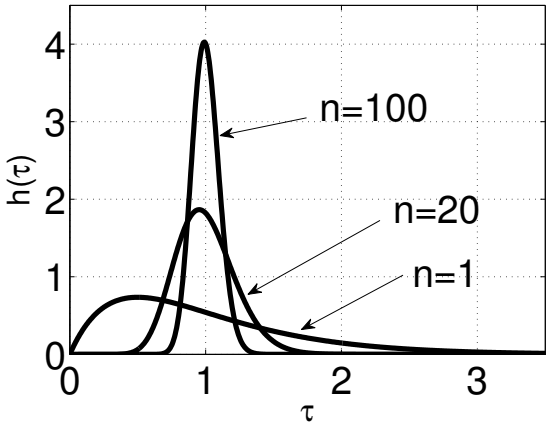

Figure 2.1: Graphs of $h(\tau)$ at $T = 1$ for $n = 1, 20, 100$.

We can exploit the convolution form of (2.5) and turn it into a differential equation for $r(t)$. Taking a Laplace Transform, we have, for the case of Lorentzian $g(\omega)$,

$$\bar{r}(s) = H(s)\bar{a}^*(s), \tag{2.15}$$

where $\bar{r}(s)$ and $\bar{a}(s)$ are the Laplace transform of $r(t)$ and $a(t)$ respectively, while

$$H(s) = [(T/\beta_n)s + 1]^{-(n+1)}, \tag{2.16}$$

is the Laplace transform of $h(\tau)$. Our choice of the function class given by Eq. (2.12) is motivated by the fact that it yields a particularly convenient Laplace transform and corresponding time-domain formulation. In particular, transforming back to

the time-domain by letting $s \to d/dt$, Eq. (2.15) yields

$$[(T/\beta_n)(d/dt) + 1]^{n+1}\, r(t) = a^*(t). \tag{2.17}$$

Thus, we now have Eqs. (2.11) and (2.17) as our description for the dynamics on the invariant manifold with heterogeneous link delays. Here, it is noteworthy that Eqs. (2.11) and (2.17) form a system of ordinary differential equations in comparison with the original system Eq. (2.1) which comprises a very large number of time-delay differential equations. Note that for the case of uniform delay, $h(\tau) = \delta(\tau - T)$, we take the limit $n \to \infty$, in which case Eq. (2.15) takes the form $\bar{r}(s) = e^{-sT}\bar{a}^*(s)$, yielding $r(t) = a^*(t - T)$, which, when substituted into Eq. (2.11), gives the time-delay differential equation for $a(t)$ in Ref. [53].

2.3 The incoherent state solution and its stability

A trivial exact solution to the system (2.11) and (2.17) is given by $r(t) = a(t) = 0$, which we refer to as the "incoherent state" [1]. Stability of the incoherent state can be studied by linearizing Eq. (2.11) about the solution $a(t) = 0$ and setting $a(t) = a_0 e^{st}$, from which we obtain

$$1 = [kH(s)/2](s + i\omega_0 + \Delta)^{-1}. \tag{2.18}$$

The critical coupling k_c at which a stable incoherent state solution becomes unstable as k increases through k_c, corresponds a solution to Eq. (2.18) with $\mathrm{Re}(s) = 0$.

The solid curves in Fig. 2.2 show results obtained from Eq. (2.18) with

[1] Note that for $r(t) = 0$, Eq. (2.4) implies that the oscillators do not interact, and run freely at their natural frequencies whose spread leads to a uniform distribution in phase.

Lorentzian $g(\omega)$ for the critical coupling value k_c versus T at different n's with parameters $\omega_0 = 3$ and $\Delta = 1$. For the case of uniform delays ($n \to \infty$), k_c as a function of T exhibits the type of dependence found in Ref. [69] with characteristic "resonances". However, as the relative spread $\delta\tau/T$ is increased (n is decreased), we see that the resonant structure that applies for the case of zero spread is strongly modified. For example, even at the relatively small spread of $\delta\tau/T \approx 0.1$ (corresponding to $n = 100$), there is only one peak (at $T \approx 1$) and one minimum (at $T \approx 2$), with k_c for $T > 2$ being very substantially higher than in the case of no spread. For $\delta\tau/T \approx 0.302$ ($n = 10$) the effect is even more severe, and the previous resonant structure is completely obliterated. For comparison, the dashed curves in Fig. 2.2 show results for $\delta\tau/T \approx 0.302$ (upper) and 0 (lower) when $g(\omega)$ is Gaussian with the same peak value as for the Lorentzian distribution used to obtain the solid curves [2]. The Gaussian and Lorentzian results are similar, suggesting that the qualitative behavior does not depend strongly on details of $g(\omega)$.

2.4 Bistable behaviors

As reported in Ref.[69], bistable behavior can exist; i.e., a situation in which both incoherent and coherent states are stable. In Figs. 2.3(a) and 2.3(b) we show the hysteresis loops obtained by numerical solution of Eqs. (2.11) and (2.17) for $n < \infty$ and, for $n = \infty$, where the $n = \infty$ result is obtained by solution of the delay

[2] In the Gaussian case the term $(s + i\omega_0 + \Delta)^{-1}$ in Eq. (2.18) is replaced by $(i\sqrt{2}\sigma)^{-1}Z(\zeta)$, where $\zeta = (\omega_0 + is)/(\sqrt{2}\sigma)$, $\sigma = \langle(\omega - \omega_0)^2\rangle$, and $Z(\zeta)$ is the "plasma dispersion function" (see http://farside.ph.utexas.edu/teaching/plasma/ lectures/node82.html).

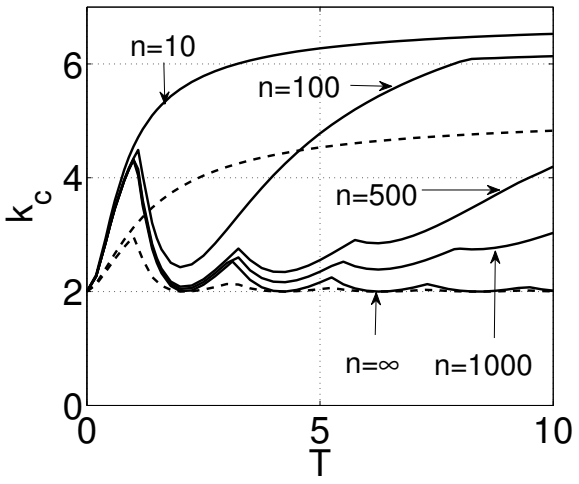

Figure 2.2: Solid curves are plots of the critical value of k_c versus T for Lorentzian $g(\omega)$ with $\omega_0 = 3, \Delta = 1$, and $n = 10, 100, 500, 1000, \infty$, corresponding to $\delta\tau/T \approx 0.302, 0.1, 0.045, 0.032, 0$. The dashed curves are for Gaussian $g(\omega)$ as described in the text.

equation obtained by inserting $r(t) = a^*(t - T)$ in (2.11). Comparing Fig. 2.3(a), which is for $T = 1$, with Fig. 2.3(b), which is for $T = 3$, we note the striking result that, for large T, hysteresis is sustained only with large enough spread in the delay distribution, i.e., when n is small [e.g., for $n = \infty$ and $T = 3$ (Fig. 2.3(b)) the bifurcation is supercritical and hysteresis is absent].

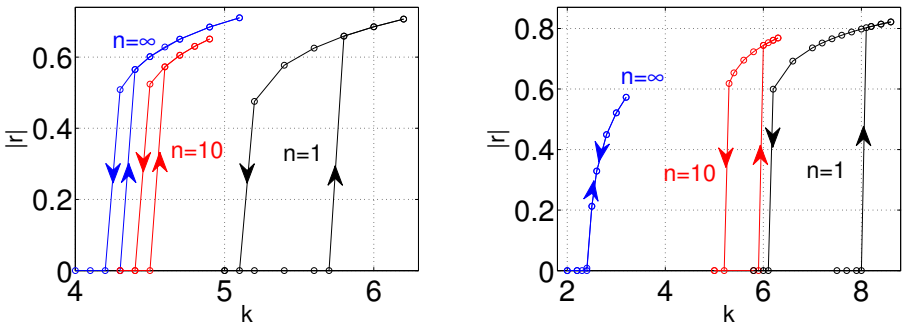

(a) (b)

Figure 2.3: Hysteresis loop at $\omega_0 = 3$, $\Delta = 1$, (a) for $T = 1$, (b) for $T = 3$.

2.5 The coherent state solution and its stability

Coherent oscillatory states can be obtained by substituting the ansatz $a(t) = a_0 e^{i\Omega t}$, where a_0 and Ω are real constants, into Eq. (2.10) and (2.11). This gives

$$[i(\Omega + \omega_0) + \Delta] + (k/2)\left(a_0^2 H^*(i\Omega) - H(i\Omega)\right) = 0,$$
$$r(t) = a_0 e^{-i\Omega t} H^*(i\Omega). \tag{2.19}$$

As reported in both [69] and [10], for $h(\tau) = \delta(\tau - T)$, multiple branches of coherent state solutions are possible in Eq.(2.19). Furthermore, we can employ Eqs. (2.11) and (2.17) to study the stability of each coherent state by introducing a small perturbation $\delta a(t)e^{i\Omega t}$ to the coherent state solution in (2.19), with $\delta a(t) = K_1 e^{st} + K_2 e^{s^* t}$. This yields the following equation for s:

$$\begin{aligned}&[s - \tfrac{k}{2}H(s + i\Omega) + A][s - \tfrac{k}{2}H(s - i\Omega) + A^*] \\ &= \left(ka_0^2/2\right)^2 H(s - i\Omega)H(s + i\Omega),\end{aligned} \tag{2.20}$$

where $A = \Delta + i(\omega_0 + \Omega) + ka_0^2 H(-i\Omega)$. Instability of each coherent state is then determined by whether there are solutions to (2.20) for s with positive real parts.

In Fig. 2.4(a) we compare the theoretical results for $|r|$ calculated from Eqs. (2.19) and (2.20) with simulation results based on Eq. (2.1) with $N = 100$ and $\delta\tau/T \approx 0.1$ ($n = 100$) for the first two branches of coherent states with $\omega_0 = 3, \Delta = 0.1, T = 1$. The solid (dashed) curves correspond to stable (unstable) coherent states. The Eq. (2.1) simulation values reported in the figures represent time averages of these quantities computed after the solution has apparently settled into the coherent state. It is seen that there is good agreement between the theory and simulations using Eq. (2.1). In addition, on simulating these two branches of coherent states, we verified that the finding of Ref. [10] that the basin of attraction is large for the first branch, but small for the second one, also holds with heterogeneous delays.

Furthermore, the number of coherent attractors strongly depends on the spread in delay times. Figure 2.4(b) shows the dependence of the number of coherent attractors on the relative delay spread $\delta\tau/T = (n+1)^{-1/2}$, with $k = 40, \omega_0 = 0, T = 1$, for two values of the frequency spread, $\Delta = 5$ (dashed) and $\Delta = 10$ (solid) (for which $k_c = 10$ and 20, respectively). For both cases, it is seen that as the relative delay spread is increased ($(n+1)^{-1/2}$ is increased), the number of coherent attractors decreases. And there remains at least one such attractor when n approaches unity, while a parameter dependent maximum is attained when $n \to \infty$, which we find is generally larger for smaller Δ and larger k [3].

[3] Kim et al. [23] (and reference therein) propose that the presence of many attractors in a Kuramoto-like model with delay (uniform delay in their treatment) can serve as a mechanism for information storage in the nervous system.

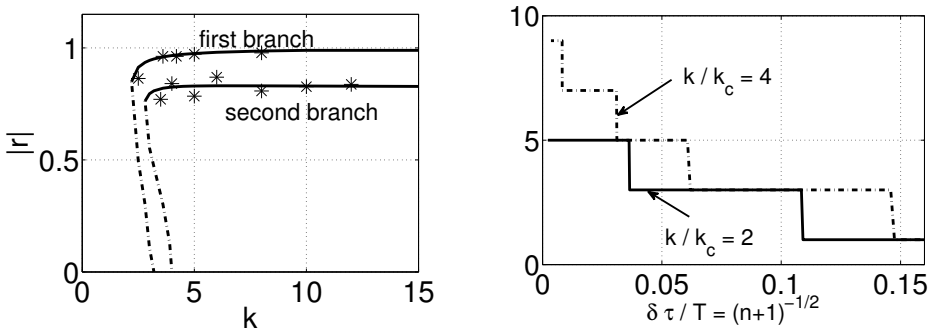

(a) (b)

Figure 2.4: (a) Magnitude of r for the first two branches of coherent states with parameter values: $\omega_0 = 3, \Delta = 0.1$, $n = 100, T = 1$ for $h(\tau)$. Solid lines give the theoretical values of the stable coherent states, dashed lines give the unstable coherent states, and asterisks give the simulation results. (b) Number of coherent attractors (number of solutions of Eq. (2.19) that are stable according to (2.20)) versus $\delta\tau/T$ for the following parameters: $k = 40, T = 1, \omega_0 = 0$; $\Delta = 10$ for the solid line ($k_c = 20$), $\Delta = 5$ for the dashed line ($k_c = 10$).

2.6 Conclusions

In conclusion, in this chapter we address, for the first time, the effect of heterogeneous delays on the dynamics of globally coupled phase oscillators. As compared to the case of uniform delay (Refs. [69, 10, 23, 43]), we find that delay heterogeneity can have important consequences, among which are the following: (i) decrease in resonant structure of the dependence of k_c on T (Fig. 2.2); (ii) increase of k_c (Fig. 2.2); (iii) enhancement of hysteretic effects (Figs. 2.3(a) and 2.3(b)); (iv) reduction in the number of coherent attractors (Fig. 2.4(b)). Furthermore, we have introduced

a framework for the study of delay heterogeneity that can be readily applied to a variety of extensions of the continuum limit ($N \to \infty$) Kuramoto model, such as communities of oscillator populations with different community dependent characteristics [7, 42], non-monotonic $g(\omega)$ [34], and periodic driving [5] (see Ref. [53] for more examples).

Chapter 3

Dynamics and pattern formation of large systems of spatially-coupled oscillators with finite response times

3.1 Introduction

In this chapter, we consider applications in which the oscillators are distributed spatially, and interact with oscillators in the local neighborhood. In particular, we seek to uncover the spatio-temporal dynamics of a system of coupled oscillators with heterogeneous oscillator response times. We first give a microscopic description of the individual oscillators and their couplings. We then spatially coarse-grain this description and use the methods developed in Ref. [30] and Chapter 2 (also Ref. [31]) to derive a set of partial differential equations giving a macroscopic description of the system dynamics. Using our derived macroscopic equations, we then numerically explore the spatio-temporal dynamics and resulting pattern formation in

both one- and two-dimensions. We find that a rich variety of behaviors are induced by the presence of time delay in the oscillator response. These include hysteresis, propagating fronts, spots, target patterns, chimerae [2, 28, 30, 62], spiral waves, etc. Related work on one dimensional spatial patterns of a spatially one dimensional oscillator system with local time delayed coupling appears in Ref. [60].

3.2 Formulation

We consider a system of N spatially distributed interacting phase oscillators with time delays between the response of an oscillator and the signal it receives. The evolution equation of oscillator m is

$$\begin{aligned}\frac{d}{dt}\theta_m(t) &= \omega_m + \sum_{n\neq m}^{N} \hat{K}_{mn} \{\sin[\theta_n(t-\tau_{mn}) - \theta_m(t)]\} \\ &= \omega_m + \sum_{n\neq m}^{N} \hat{K}_{mn} \frac{1}{2i} \{e^{-i[\theta_m(t)-\theta_n(t-\tau_{mn})]} - c.c.\}, \end{aligned} \tag{3.1}$$

where $\hat{K}_{mn}$ is the interaction strength between oscillators m and n, which is assumed to be spatial in character (i.e., $\hat{K}_{mn}$ becomes small or zero if the distance between oscillator m and oscillator n is large), τ_{mn} is the interaction time delay in the effect of oscillator n on oscillator m, and *c.c.* denotes complex conjugate.

Assuming a separation in the scales of the macroscopic and microscopic system dynamics, we follow a path similar to that employed by kinetic theory to reduce the study of a gas of many interacting molecules to a fluid description. We begin by partitioning the continuous space into discrete regions $I_{\bar{x}}$ centered at the discrete set of spatial points $\bar{x}$, such that the domain of interest is $\cup_{\bar{x}} I_{\bar{x}}$, and $I_{\bar{x}} \cap I_{\bar{x}'} = \emptyset$ for $\bar{x} \neq \bar{x}'$. The diameter of each region is $|I_{\bar{x}}| \sim w$, and the volume of each region is

w^d where d denotes the dimension of space.

These regions are assumed to be small enough that $\hat{K}_{mn} \approx \hat{K}_{ml}$ if oscillators n and l are in the same region $I_{\bar{x}'}$, yet large enough that many oscillators ($N_{I_{\bar{x}'}} \gg 1$) are contained within each $I_{\bar{x}'}$. Thus we can meaningfully define

$$\begin{aligned} \rho(\bar{x}') &\equiv \frac{N_{I_{\bar{x}'}}}{w^d}, \\ r(\bar{x}', t) &\equiv \frac{1}{N_{I_{\bar{x}'}}} \sum_{n \in I_{\bar{x}'}} e^{i\theta_n(t)}, \end{aligned} \tag{3.2}$$

respectively as the local density and the local order parameter in $I_{\bar{x}'}$. In addition, for all $m \in I_{\bar{x}}$ and $n \in I_{\bar{x}'}$, we approximate $\hat{K}_{mn} \approx K_{\bar{x}\bar{x}'}$. The summation in (3.1) can thus first be approximated as

$$\frac{1}{2i} \left[\sum_{I_{\bar{x}'}} K_{\bar{x},\bar{x}'} N_{I_{\bar{x}'}} e^{-i\theta_m(t)} \frac{1}{N_{I_{\bar{x}'}}} \sum_{n \in I_{\bar{x}'}} e^{i\theta_n(t-\tau_{mn})} - c.c. \right]. \tag{3.3}$$

In all of what follows, we consider only the simple illustrative case that $\tau_{mn} = \tau_m$, i.e., we suppose that the delay in the effect of oscillator n upon oscillator m is independent of n. This would, e.g., apply if the signal propagation time from n to m was very fast, but each oscillator had a finite reaction time. Together with Eq. (3.2), Eq. (3.3) can then be written as

$$\sum_{I_{\bar{x}'}} w^d K_{\bar{x}\bar{x}'} \rho(\bar{x}') \mathrm{Im}\{e^{-i\theta_m(t)} r(\bar{x}', t - \tau_m)\}. \tag{3.4}$$

Since we assume $N_{I_{\bar{x}}} \gg 1$ for all $\bar{x}$, it is appropriate to introduce a distribution function $F(\theta, \omega, \bar{x}, \tau, t)$ proportional to the fraction of oscillators in $I_{\bar{x}}$ with $\theta \in [\theta, \theta + d\theta]$, $\omega \in [\omega, \omega + d\omega]$ and $\tau \in [\tau, \tau + d\tau]$ at time t. We furthermore pass to the limit of continuous space by replacing the discrete variable $\bar{x}$ by a new variable x

which we now regard as continuous. In terms of this distribution, we introduce the marginal distribution $\hat{g}(\omega, \tau, x)$,

$$\hat{g}(\omega, \tau, x) = \int_0^{2\pi} F(\theta, \omega, \tau, x, t) d\theta. \tag{3.5}$$

Here, note that since ω, τ and x for any oscillator are assumed to be constant in time, the $\theta-$integral of F is time independent even though F itself depends on time. With Eq. (3.5), the quantity r in Eq. (3.2) becomes

$$\begin{aligned} r(x,t) &= \frac{\int_0^\infty \int_{-\infty}^\infty \int_0^{2\pi} F(\theta, \omega, \tau, x, t) e^{i\theta} d\theta d\omega d\tau}{\int_0^\infty \int_{-\infty}^\infty \int_0^{2\pi} F(\theta, \omega, \tau, x, t) d\theta d\omega d\tau} \\ &= \frac{1}{\rho(x)} \int_0^\infty \int_{-\infty}^\infty \int_0^{2\pi} F(\theta, \omega, \tau, x, t) e^{i\theta} d\theta d\omega d\tau \end{aligned} \tag{3.6}$$

The overall system dynamics can be studied in terms of the evolution equation for $F(\theta, \omega, \tau, x, t)$,

$$\frac{\partial F}{\partial t} + \frac{\partial}{\partial \theta} \left(F\{\omega + \mathrm{Im}[\eta(x, t-\tau) e^{-i\theta}]\} \right) = 0, \tag{3.7}$$

where

$$\eta(x,t) = \int \rho(x') K(x, x') r(x', t) dx' \tag{3.8}$$

is Eq. (3.4) in the continuum limit, and the integration in (3.8) is over the d-dimensional spatial domain. Referring back to our previous analogy to kinetic theory of a gas, we think of Eqs. (3.7) and (3.8) as a kinetic description roughly analogous to the Boltzmann equation.

To proceed we wish to reduce our kinetic description (3.7) and (3.8) to a PDE (partial differential equation) system analogous to the fluid equations of gas

dynamics. We do this using the recent work of Ott and Antonsen (Refs. [53]-[54]). We expand F in a Fourier series of the form

$$F(\theta,\omega,\tau,x,t)=\frac{\hat{g}(\omega,\tau,x)}{2\pi}\left\{1+\left[\sum_{n=1}^{\infty}f_n(\omega,\tau,x,t)e^{in\theta}+c.c.\right]\right\}. \tag{3.9}$$

As discussed and justified in Refs. [53] and [54], we seek a solution in the form

$$f_n(\omega,\tau,x,t)=\hat{\alpha}(\omega,x,t-\tau)^n. \tag{3.10}$$

Equations (3.6) to (3.8) then yield

$$\begin{aligned}\frac{\partial}{\partial t}\hat{\alpha}(\omega,x,t-\tau)+i\omega\hat{\alpha}(\omega,x,t-\tau)\\ +\frac{1}{2}\left[\eta(x,t-\tau)\hat{\alpha}^2(\omega,x,t-\tau)-\eta^*(x,t-\tau)\right]=0,\end{aligned} \tag{3.11}$$

$$\eta(x,t-\tau)=\int\rho(x')K(x,x')r(x',t-\tau)dx', \tag{3.12}$$

$$r(x,t)=\int\frac{1}{\rho(x)}\int_{-\infty}^{\infty}\hat{g}(\omega,\tau',x)\hat{\alpha}^*(\omega,x,t-\tau')d\omega d\tau', \tag{3.13}$$

where the star * denotes complex conjugate, and τ' is written inside Eq. (3.13) to emphasize its role as a dummy integration variable as compared with τ's in the other equations.

In what follows, we study an illustrative case corresponding to

$$\hat{g}(\omega,\tau,x)=g(\omega)h(\tau)\rho_0, \tag{3.14}$$

$$K(x,x')=kq(x-x'), \tag{3.15}$$

where $\int_{-\infty}^{\infty}g(\omega)d\omega=\int_0^{\infty}h(\tau)d\tau=1$. Equation (3.14) implies that the oscillator frequencies, locations, and delay distributions are uncorrelated, and that the oscillator density ρ_0 is uniform. Equation (3.15) states that the strength of the coupling

between oscillators at two points depends uniformly on their spatial separation. Further, in (3.15) we take $q(x)$ to be suitably normalized, so that the constant k may be regarded as an overall coupling strength. With these assumptions, together with the transformation $t \to t + \tau$ in Eqs. (3.11) and (3.12), and rewriting τ' as τ in Eq. (3.13), we obtain

$$\frac{\partial}{\partial t}\hat{\alpha}(\omega, x, t) + i\omega\hat{\alpha}(\omega, x, t) + \frac{k}{2}\left[\eta(x, t)\hat{\alpha}^2(\omega, x, t) - \eta^*(x, t)\right] = 0, \tag{3.16}$$

$$\eta(x, t) = \int \rho_0 q(x - x')r(x', t)dx', \tag{3.17}$$

$$r(x, t) = \int \left[\int_{-\infty}^{\infty} g(\omega)\hat{\alpha}^*(\omega, x, t - \tau)d\omega\right] h(\tau)d\tau. \tag{3.18}$$

In order to reveal generic expected behavior, we now further specify particular convenient choices for the frequency distribution, $g(\omega)$, the response time distribution, $h(\tau)$, and the spatial interaction kernel, $q(x)$.

We assume a Lorentzian form for $g(\omega)$,

$$\begin{aligned} g(\omega) &= \frac{\Delta/\pi}{(\omega - \omega_0)^2 + \Delta^2} \\ &= \frac{1}{2\pi i}\left\{\frac{1}{\omega - \omega_0 - i\Delta} - \frac{1}{\omega - \omega_0 + i\Delta}\right\}. \end{aligned} \tag{3.19}$$

Assuming $\hat{\alpha}$ is analytic in ω, we close the $\omega-$integration path in (3.18) with a large semi-circle of radius $R \to \infty$ in the lower half complex $\omega-$plane. Thus we obtain from the pole of $g(\omega)$ at $\omega = \omega_0 - i\Delta$ [see Eq. (3.19)],

$$r(x, t) = \int \alpha^*(x, t - \tau)h(\tau)d\tau, \tag{3.20}$$

where $\alpha(x, t) = \hat{\alpha}(\omega_0 - i\Delta, x, t)$, and we have assumed (Ref. [53]) that, as $\mathrm{Im}(\omega) \to -\infty$, $\hat{\alpha}(\omega, x, t)$ is sufficiently well-behaved that the contribution from the integration

over the large semicircle approaches zero as $R \to \infty$. Setting $\omega = \omega_0 - i\Delta$ in Eq. (3.16) we obtain the following equation for the time evolution of $\alpha(x,t)$,

$$\frac{\partial}{\partial t}\alpha(x,t) + (\Delta + i\omega_0)\alpha(x,t) + \frac{k}{2}\left[\eta(x,t)\alpha^2(x,t) - \eta^*(x,t)\right] = 0. \tag{3.21}$$

Our assumed form for the response time distribution $h(\tau)$ is given in Chapter [**?**] (also Ref. [31]),

$$h_n(\tau) = A_n \tau^n e^{-\beta_n \tau}, \tag{3.22}$$

where A_n and β_n are defined by $\int_0^\infty h(\tau)d\tau = 1$ and $\int_0^\infty \tau h(\tau)d\tau = T$. Noting the convolution form of Eq. (3.20), we can re-express (3.20) as

$$\left(\frac{T}{n+1}\frac{\partial}{\partial t} + 1\right)^{n+1} r(x,t) = \alpha^*(x,t). \tag{3.23}$$

For the interaction kernel, we choose $q(x)$ to be the solution to the problem,

$$\left(\nabla^2 - \frac{1}{L^2}\right) q(x) = -\frac{1}{L^2}\delta(x). \tag{3.24}$$

For example, for an unbounded domain with boundary conditions $q(x) \to 0$ as $|x| \to \infty$, we obtain

$$q(x) = \begin{cases} \frac{1}{2L}\exp\left(-\frac{|x|}{L}\right) & \text{for } d = 1, \\ \frac{1}{2\pi L^2} K_0\left(\frac{|x|}{L}\right) & \text{for } d = 2, \\ \frac{1}{4\pi|x|L^2}\exp\left(-\frac{|x|}{L}\right) & \text{for } d = 3, \end{cases} \tag{3.25}$$

where $K_0(|x|/L)$ is a zero order Bessel function of imaginary argument. Using Eq. (3.24), Eq. (3.17) can be rewritten by acting on it with the operator $(\nabla^2 - \frac{1}{L^2})$,

giving

$$\nabla^2\eta(x,t) - \frac{1}{L^2}\eta(x,t) = -\frac{1}{L^2}\rho_0 r(x,t) \tag{3.26}$$

Thus we obtain a closed system of three PDE's in the independent variables x and t given by Eq. (3.21) for $\alpha(x,t)$, Eq. (3.23) for $r(x,t)$, and Eq. (3.26) for $\eta(x,t)$. In the rest of this chapter we study solutions of these equations in one- and two-dimensional domains of size D with periodic boundary conditions. The parameters of this system are

$$\Delta, \omega_0, k, L, T, D, \rho_0, n.$$

By suitable normalization we can remove three of these parameters. We will do this by redefining η and k to absorb ρ_0 and by normalizing time to Δ^{-1} and distance to L. This can also be viewed as using our original parameter set with the choices $\Delta = 1, L = 1, \rho_0 = 1$. In either case, our normalized PDE description becomes

$$\frac{\partial}{\partial t}\alpha(x,t) + (1 + i\omega_0)\alpha(x,t) + \frac{k}{2}\left[\eta(x,t)\alpha^2(x,t) - \eta^*(x,t)\right] = 0, \tag{3.27}$$

$$\left(\frac{T}{n+1}\frac{\partial}{\partial t} + 1\right)^{n+1} r(x,t) = \alpha^*(x,t), \tag{3.28}$$

$$(\nabla^2 - 1)\eta(x,t) = -r(x,t). \tag{3.29}$$

In addition, in what follows we will only consider $n = 0$ corresponding to $h(\tau) = T^{-1}\exp(-\tau/T)$. Thus, our reduced parameter set is

$$\omega_0, k, T, D. \tag{3.30}$$

Before turning to the study of Eqs. (3.27)-(3.29), we briefly comment on the analogy of the derivation of our evolution equations (3.27)-(3.29) to the derivation of the equations of gas dynamics from Boltzmann's equation. Substituting (3.10)

into (3.9) and summing the geometric series ($|\hat{\alpha}| < 1$ is assumed for convergence), we obtain

$$F(\theta, \omega, x, \tau, t) = \frac{\hat{g}(\omega, x, \tau)}{2\pi} \left(\frac{1 - |\hat{\alpha}|^2}{1 + |\hat{\alpha}|^2 - 2|\hat{\alpha}| \cos(\theta - \psi)} \right), \tag{3.31}$$

where $\hat{\alpha} = |\hat{\alpha}| \exp(-i\psi)$. It is shown in Refs. [53] and [54] that, under very general conditions, the solution to our Eq. (3.7) relaxes to this form. In gas dynamics, the solution to Boltzmann's equation, via the Chapman-Enskog expansion (Ref. [9]), is assumed to approximately relax to a local Maxwellian distribution whose velocity-space width is controlled by the temperature, and whose velocity-space maximum is located at the fluid velocity. In analogy with this situation, Eq. (3.31) is peaked in θ (analogous to velocity space) at the location $\theta = \psi$ (analogous to the fluid velocity), and the width of this peak is controlled by $|\hat{\alpha}|$ (analogous to temperature) with F becoming a delta function in θ as $|\hat{\alpha}| \to 1$ (analogous to temperature $\to 0$). In contrast to the derivation of gas dynamics from the Boltzmann equation, our relaxation to (3.31) is due to the phase mixing of many oscillators with different natural frequencies, whereas relaxation to a local Maxwellian in gas dynamics is due to chaos in the collisional dynamics of interacting particles. Another difference is that (3.31) is an exact, rigorous result (as shown in Refs. [54] and [55]), while relaxation to a local Maxwellian in the derivation of gas dynamics is an asymptotic result in the ratio of the mean free path (and mean free time) to the macroscopic length (and time) scale.

3.3 Numerical studies and discussions

3.3.1 1D propagating fronts, "bridge" and "hole" patterns

The simplest solutions of our system, Eqs. (3.27)-(3.29), are the homogeneous incoherent state solution ($r = 0$ everywhere) and the homogeneous coherent state solution ($r = r_0 e^{i\Omega t}$ where r_0 and Ω are real constants). As shown in Refs. [69, 10] and Chapter 2 (also Ref. [31]) for the case of globally coupled oscillators [corresponding to $\nabla^2 \to 0$ in Eq. (3.29)], a distribution of interaction time-delays induces bistability and hysteretic behaviors. Figure 3.1 shows an example of the hysteresis loop in the $|r| - k$ plane for spatially homogeneous states with $\omega_0 = 5, T = 1$, which is obtained by solving Eqs. (3.27) to (3.29) with $\eta = r$ for the coherent solution $r = r_0 e^{i\Omega t}$.

We first consider a one-dimensional version of our system, Eqs. (3.27)-(3.29), for a k value within the bistable region, $k = 12$, and examine the evolution resulting from several initialized configurations with different spatial regions in the homogeneous incoherent and coherent state solutions. Results are shown in Fig. 3.2. Note that the final state is either coherent or incoherent depending on how large the initial incoherent region is. Thus, there appears to be a critical initial size of the incoherent region beyond which the incoherent region takes over. Furthermore, from Fig. 3.2, we see that the evolutionary process leading to this final state is by propagation of fronts separating coherent and incoherent regions, and that these fronts propagate at an approximately constant speed. In addition to this initial example, we find a variety of other one-dimensional spatio-temporal behaviors to be reported in the

following.

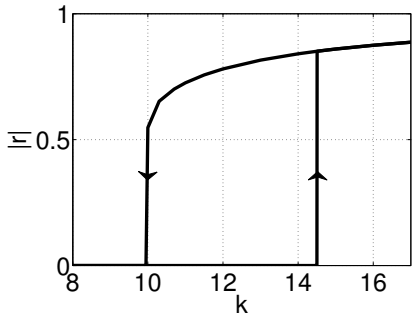

Figure 3.1: Hysteresis loop for $\omega_0 = 5, T = 1$. The upper and lower branches correspond to stable coherent and incoherent states.

Next, we consider the dynamics as a function of the coupling strength k. Recall from Fig. 3.1 that there is a hysteretic region of coexisting coherent and incoherent states for the region $k_c' < k < k_c$ where $k_c' = 10$ and $k_c = 14.5$. Figure 3.3 shows the time evolution of $|r(x,t)|$ as a function of k. When the state is initialized with half ($25 \leq x \leq 75$) the domain in the homogeneous incoherent state and the remaining half in the homogeneous coherent state, it is seen that if k is sufficiently close to k_c', then the incoherent region engulfs the coherent region, while if k is sufficiently greater than k_c, the homogeneous coherent solution takes over, and by comparing Figs. 3.3(a) to 3.3(e), we find that the propagation velocity decreases as k is increased toward k_c. As k increases past $k \sim 12$, the simple propagating front phenomenon seen in Figs. 3.2 and 3.3(a)-3.3(c) is replaced by more complex behavior. For example, in Fig. 3.3(d) we observe the formation of a "bridge" at $k = 13$ ($< k_c$), i.e., a narrow stable coherent region sandwiched between two broad

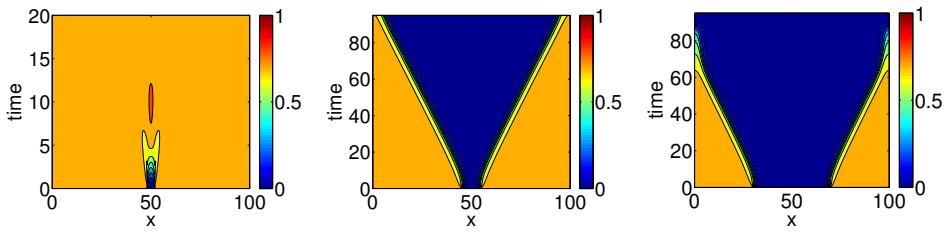

(a) (b) (c)

Figure 3.2: $|r(x,t)|$ for, (a) an initial configuration with a small part of the one-dimensional spatial domain in the incoherent state (blue) and a large part in the coherent state (orange), (b) a larger part of the spatial domain is initially in the incoherent state than that in (a), and (c) a still larger initial incoherent region. ($\omega_0 = 5, T = 1, D = 100, k = 12$).

incoherent regions. This solution is apparently a long-time stable state. It develops as the two propagating fronts collapsing the coherent regions slow to a halt as they approach each other. We note further that the bridge has an amplitude which is smaller than that of the stable homogeneous solution, and the oscillation frequency is different as well (graphs not shown). Further, this bridge type solution persists for $k > k_c$, and can give rise to further intriguing dynamics like multiple bridges, as shown in Figs. 3.3(g), and even more vigorous behaviors of merging and re-creation of plateaus of coherent regions and bridges, as seen in Fig. 3.3(h). Comparing Fig. 3.3(f) to 3.3(h), it is notable that a wide variety of evolutionary behaviors occurs within a relatively small range in k, including the formation of single and multiple bridges, as well as collapse and re-creation of plateaus. Figure 3.4 studies the glassy-like behavior related to that seen in Fig. 3.3(h) at a slightly different set of

system parameters. The figure shows plateaus of coherent regions (orange triangles in Figs. 3.4(a) and 3.4(b)) and bridge-like patterns (yellow stripes), connected through dynamical creation, merging and re-creation of such structures until the system eventually evolves into the homogeneous coherent state. Figure 3.4(c) shows the phase evolution inside the plateau region (orange triangle) of Fig. 3.4(a) centered at $t \approx 420, x \approx 50$. Figure 3.4(d) shows the phase evolution corresponding to the four-bridge-structure between the top of Fig. 3.4(a) and the bottom of Fig. 3.4(b) ($700 \leq t \leq 1300$). We note that within a plateau, the whole region oscillates roughly homogeneously (see the nearly parallel evolving fronts in Fig. 3.4(c)), and each bridge pattern functions as a sink of incoming waves (see the zig-zag-like pattern in Fig. 3.4(d)). Further important dynamical characteristics during this vigorous glassy-like transition state are revealed in Figs. 3.4(e) and 3.4(f), which show $|r|$ and θ (where $r = |r|e^{i\theta}$) respectively at $t = 148$. We see that there are multiple hole-like patterns (deep dips in $|r|$ in Fig. 3.4(e)), at which the phase changes sharply, (see Fig. 3.4(f), and note that the changes in phase for the outer two holes appear to be virtually discontinuous, as discussed in more detail shortly). In comparison, for the multiple-bridge region at $t = 1200$, Figs. 3.4(g) and 3.4(h) show that both $|r|$ and θ change smoothly in space.

Figure 3.5 shows the dynamical characteristics associated with the hole-like patterns in another setting where these patterns dominate and are not interspersed with other spatial features (like bridges and plateaus). The figure corresponds to the same parameters as those in Fig. 3.3(h), but initialized with different incoherent and coherent regions. Compared with Fig. 3.3(h), there is a relatively short time

for the system to stay in the plateau-like regions, and instead of settling in the homogeneous coherent state solution as in Fig. 3.3(h), four distinct hole-like patterns emerge (black lines starting at $t \approx 130$ in Fig. 3.5(a)). As time evolves, the two inner holes move toward each other and annihilate, while the outer two continue to evolve, apparently becoming stationary. Note also that for the two merging holes, they approach each other at a faster speed when they are closer to each other. Examination of the phase evolution of the system (Figs. 3.5(b) and 3.5(e)) suggests the center of each hole act as a source of plane waves, in contrast with the bridge solution which acts as a sink (see Fig. 3.4(d)). For the inner two moving holes, while each is characterized by a dip in magnitude (see Fig. 3.5(c) at $t = 192$), the dips decrease in magnitude as the two holes approach each other, with the relative phase difference on the two sides of the hole center close to being continuous (see Fig.3.5(d)). However, if the holes are stationary, e.g., the outer two holes in Figs. 3.5(c) and 3.5(f), each dip in $|r|$ is close to zero, with the relative phase difference on the two sides being an essentially discontinuous slip of $\pm 3\pi$. A further observation in the case of two stationary holes is that there is a bump in $|r|$ half-way between them corresponding to the location at which incoming waves emitted from the holes converge (see $x = 50$ in Fig. 3.5(f)).

In fact, when $k \approx k_c$, the hole-like pattern is a feature that shows up readily when two plane waves with a relative phase difference of $\pm\pi$ (or odd-multiples of them) collide. An example is studied in Fig. 3.6 where two waves of relative phase difference π collide giving rise to a hole pattern. This observation is consistent with the relative phase differences observed at the two outer holes studied in Fig. 3.5(g).

Furthermore, although the hole pattern seems to arise only under relatively specific conditions, it is found to be pretty stable with respect to changes in parameters or small perturbations once it is formed. Finally, as shown in Fig. 3.7, we note that the hole core occupies a finite width and so is not a point singularity when $T \neq 0$. This will be shown to have a close correspondence with the spiral wave in our two-dimensional study (sec. 3.3.3).

It is further interesting to note some similarity between our observations in the region $k \approx k_c$ and the intermittency regime of the complex Ginzburg-Landau equation (CGLE) (See for example, section III of Ref. [6], and section 2.5 of Ref. [46]). There, the CGLE displays similar glassy-like transition patterns characterized by large plateaus of coherent regions with hole-like patterns being continuously created and destroyed. However, there are also differences between the two systems. For example, the CGLE does not seem to have a close counterpart to the bridge pattern observed in our system, while more intricate dynamics of hole creation and destruction leading to zigzagging holes and defect chaos have not been observed in our study.

3.3.2 2D propagating fronts and "bridge" patterns

Figures 3.8 and 3.9 show the $d = 2$ counterparts to the $d = 1$ propagating fronts and associated features. Similar to what was previously done for $d = 1$, half of the system is initialized in the homogeneous incoherent state and the remaining half in the homogeneous coherent state, and they are divided by a sinusoidally wiggling boundary (Figs. 3.8(a) and 3.9(a)). Analogous to the $d = 1$ case, for $d = 2$,

the homogeneous incoherent state and homogeneous coherent state take over when k is sufficiently small or large compared to k_c respectively. The most interesting behaviors again take place when $k \approx k_c$. With $k = 14.4 < k_c$, Fig. 3.8 shows the development of a stable bridge solution. In contrast, with $k = 14.8 > k_c$, Fig. 3.9 shows a surprisingly rich spatio-temporal pattern evolution. As in Fig. 3.8, the originally coherent half apparently starts to shrink into a bridge (see Fig. 3.9(b)); however, as time progresses further, we see that coherent regions arise out of the originally incoherent regions to form new features (see also Figs. 3.3(g) and 3.3(h) in the $d = 1$ case), and these new features interact in a nontrivial two dimensional manner. For example, when two neighboring coherent regions get close to each other, they can form bonds and merge into each other: see the connections formed between bridge-like structures from $t = 83$ to $t = 98$; also see the coherent spot formed at the upper left hand corner at $t = 245$ and see how it merges into the bridge on its right as time progresses to $t = 400$. We also observe that, during the process of merger, bridge-like structures may also temporarily separate and then re-connect: see the connecting bridge at the bottom right hand corner from $t = 138$ to $t = 170$. A further notable feature is the coherent spot on the top left hand corner at $t = 561$ (a target pattern in the phase plot as shown in the next section), which survives from $t = 561$ to the end of the numerical run. In the above reported numerical experiments we observe that both incoherent and coherent regions coexist for a long time. We do not know, however, whether a coherent or incoherent state ultimately will take over the whole domain at longer time.

3.3.3 2D Spots, spiral waves and target patterns

Figure 3.10 shows the time evolution of both $|r(\mathbf{x},t)|$ and $\sin[\theta(\mathbf{x},t)]$ [where $r(\mathbf{x},t) = |r(\mathbf{x},t)|\exp[i\theta(\mathbf{x},t)]$, and $\mathbf{x} = (x,y)$ in $2D$] when the system is initialized with a small random initial condition at each grid point, and the coupling strength is $k = 15.5$ ($> k_c = 14.5$). As expected from our previous studies, when $k > k_c$, coherent regions ($|r| \approx 1$) emerge from the initial incoherent state. Further, the phase plots show some distinct target-like patterns of nested closed surfaces of constant phase (see $t = 40$ and $t = 217$). As time progresses, coherent regions (red in the $|r|$ plots) become dominant and only small islands of incoherent regions remain (blue in the $|r|$ plots). Similar to our previous observation of propagating fronts when $k > k_c$ (compare Figs. 3.9(g) and 3.9(h)), coherent regions can form in an originally incoherent region ($|r| \ll 1$). For example, see the figures from $t = 139$ to $t = 161$, and especially from $t = 195$ to $t = 225$, where we see coherent regions (red/yellow) appearing and growing in the interior of incoherent (blue) blob, eventually destroying it. As can be inferred by comparing the $|r|$ and $\sin(\theta)$ plots, small blue, dot-like features in the $|r|$ plots represent phase defects in the complex amplitude (i.e., counter clockwise encirclement of such a feature leads to a phase change of either $+2\pi$ or -2π), and these blue dot features are commonly seen as spiral wave type patterns in the phase plots. When, as in the previously noted plots from $t = 195$ to 225, coherent regions take over from an incoherent patch, we also note that a number of phase defects result (which must be formed in opposite-spiral-parity pairs due to the conservation of topological charge); see $t = 250$. The

isolated phase defects subsequently wander about, and some of them are seen to annihilate with others of opposite parity (see the two defects closest to the bottom of the picture at $t = 267$ and their evolution up to $t = 293$), or sometimes they are absorbed into an incoherent region (e.g., compare the $|r|$ plots at $t = 195$ and $t = 217$). Lastly, regarding the speed of motion of spiral patterns, we note that similar to the observation in Fig. 3.5(a), when oppositely charged spirals get close enough to each other, their speed of approach becomes distinctively faster till they annihilate each other.

In studies of the CGLE, the hole pattern and spiral wave pattern are analogous phenomena occurring in $d = 1$ and $d = 2$, respectively. Indeed, the hole pattern and spiral wave pattern exhibit similar characteristics in our study. Both features are stable with respect to small changes in parameters, and exhibit similar dynamical characteristics of approach and annihilation as described above. In addition, Fig. 3.11 shows, in parallel with Fig. 3.7, that the central core of the spiral wave pattern occupies a finite area when $T \neq 0$. This is similar to the chimera-centered spirals noted in Refs. [35, 29].

3.3.4 2D pulsating pattern

Another class of local coherent structures supported in the $d = 2$ case is shown in Figs. 3.12 and 3.13, which shows a localized pulsating spot in an incoherent background. It is interesting to notice that oscillations of the magnitude and phase (which show up in the form of target patterns) of $r(x, t)$ are not the same, with that of the phase oscillation being more irregular and more than an order of magnitude

faster than the amplitude oscillation (Figs. 3.12(d) and 3.13(g)). It is interesting to note that for the CGLE, stable pulsating patterns come only with the addition of a quintic term (see Ref. [14], and the later work Ref. [4] and references therein).

3.4 Summary and Concluding Remarks

In this chapter, we have studied the spatio-temporal dynamics of spatially coupled oscillator systems where the oscillators have a heterogeneous distribution of response times. Using the results of Refs. [53]-[55], we have derived a macroscopic PDE description for this situation [Eqs. (3.27)-(3.29)]. The resulting macroscopic dynamics are found to exhibit a wide variety of pattern formation behaviors. We characterized the possible behaviors roughly according to the hysteresis loop corresponding to bistable homogeneous incoherent and homogeneous coherent state solutions. Numerical studies show that the system behaviors for k sufficiently below/above the bistable k-range are simple in that the homogeneous incoherent/coherent state eventually takes over the entire domain. In contrast, for k in or near the bistable range the system can exhibit a variety of interesting spatio-temporal phenomena. These include propagating fronts, bridge patterns, hole patterns ($d = 1$), spiral waves ($d = 2$), spots, target patterns, pulsating patterns, etc.

Finally, it is interesting to consider the role of time delay in contributing to the features that we observed. If there is no time delay (i.e., $T = 0$), there is no homogeneous bistable behavior as observed in Fig. 3.1, and the transition from the homogeneous incoherent state to the homogeneous coherent state is supercritical and takes place at $k_c = 2\Delta$. In this case, many of the interesting spatio-temporal

phenomena that we have found for $T > 0$ are absent. For example, when $T = 0$, the intricate 1D glassy state transitions were not observed, and the system typically evolves relatively rapidly into either homogeneous incoherent or homogeneous coherent state solutions. The 2D waves arisen from topological defects are still present; however, for $T = 0$ the system will be similar to the case of zero nonlinear dispersion in Ref. [62], where the incoherent core remains a point defect but not a finite area as observed when $T \neq 0$. Thus finite response time introduces additional dynamics, leading to the large variety of behaviors observed.

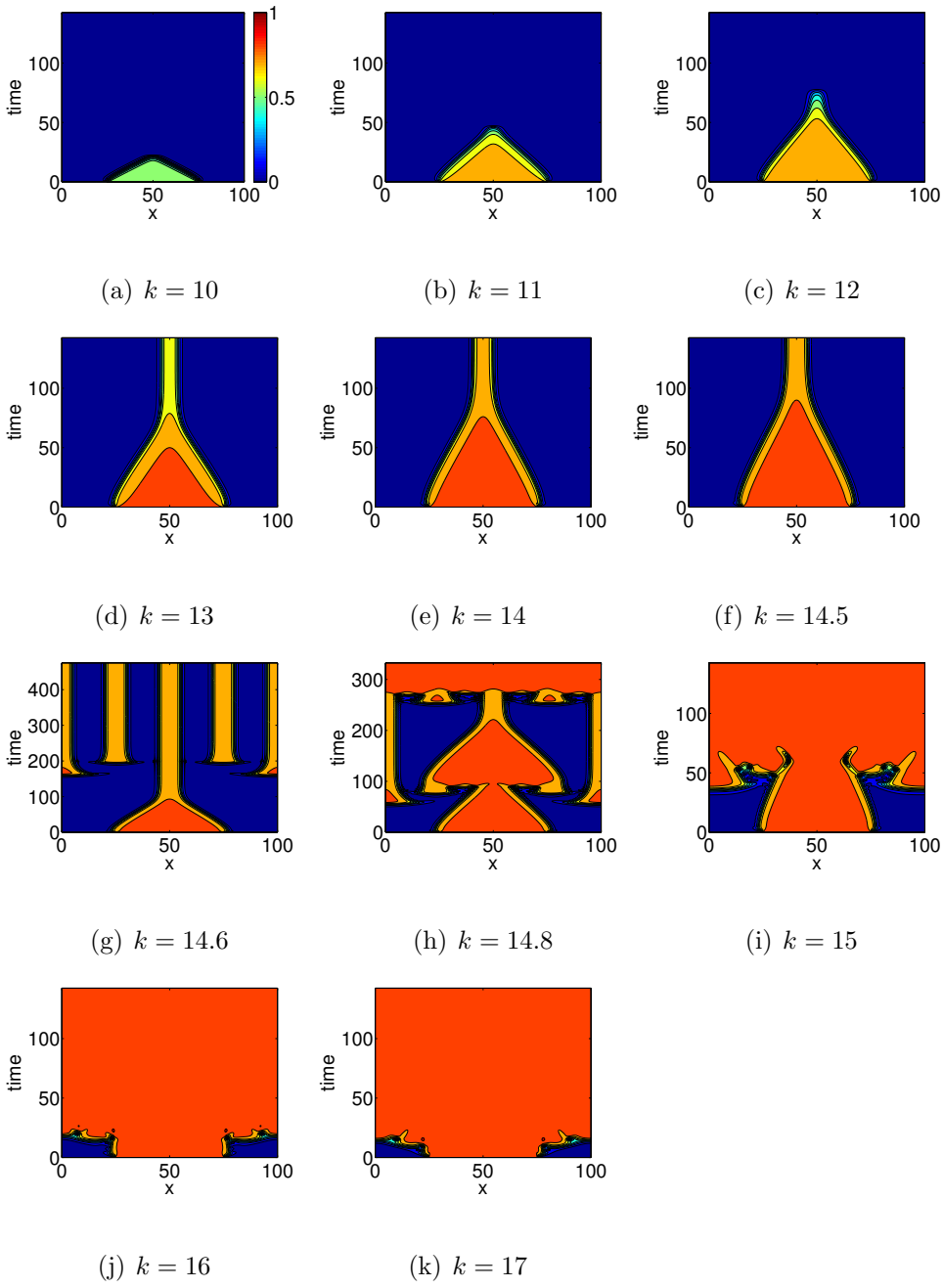

(a) $k = 10$ (b) $k = 11$ (c) $k = 12$

(d) $k = 13$ (e) $k = 14$ (f) $k = 14.5$

(g) $k = 14.6$ (h) $k = 14.8$ (i) $k = 15$

(j) $k = 16$ (k) $k = 17$

Figure 3.3: A comparison of the time evolutions of $|r(x,t)|$ for different values of k where r is initialized with half of the interval at the coherent state ($25 \leq x \leq 75$) and half at the incoherent state. Notice the difference in time scales of Fig. 3.3(g) and Fig. 3.3(h) from other figures ($\omega_0 = 5, T = 1, D = 100$; periodic boundary conditions are imposed).

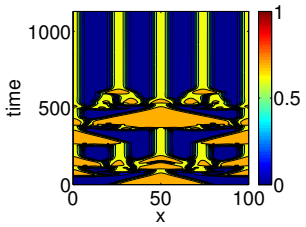

(a) $|r(x,t)|$

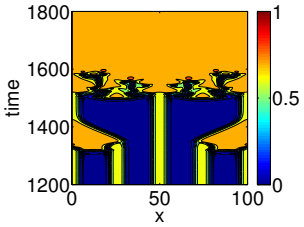

(b) $|r(x,t)|$

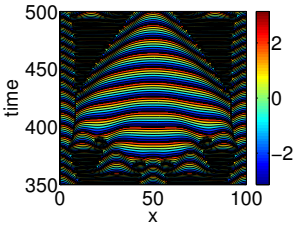

(c) $\theta(x,t)$ in the plateau centered at $x = 50$ and $t = 420$.

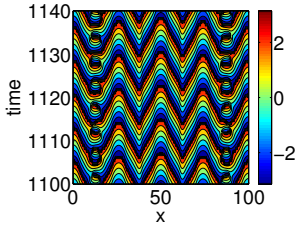

(d) $\theta(x,t)$ in part of the multiple-bridge pattern for $700 \leq t \leq 1300$.

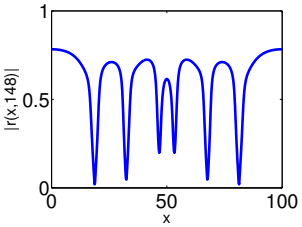

(e) $|r(x,148)|$

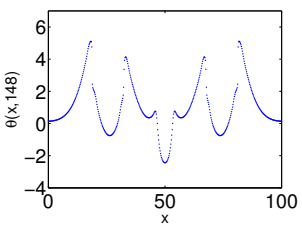

(f) $\theta(x,148)$

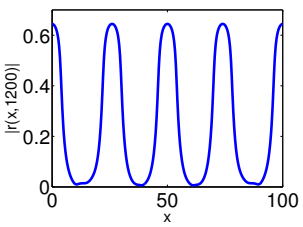

(g) $|r(x,1200)|$

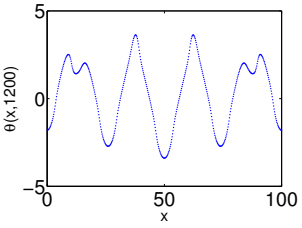

(h) $\theta(x,1200)$

Figure 3.4: (a,b) Glassy state of transition, formation of plateaus of coherent regions and hole patterns, and final evolution into the homogeneous coherent state. (c,d) Phase evolution in the plateau and multiple-bridge regions. (e,f) $|r(x,148)|$ and $\theta(x,148)$. (g,h) $|r(x,1200)|$ and $\theta(x,1200)$ ($\omega_0 = 4, T = 1, D = 100, k = 10.3\ (> k_c = 10)$; initial condition: r is given by the homogeneous coherent state solutions for $25 \leq x \leq 75$, and $r = 0$ otherwise; periodic boundary conditions are imposed).

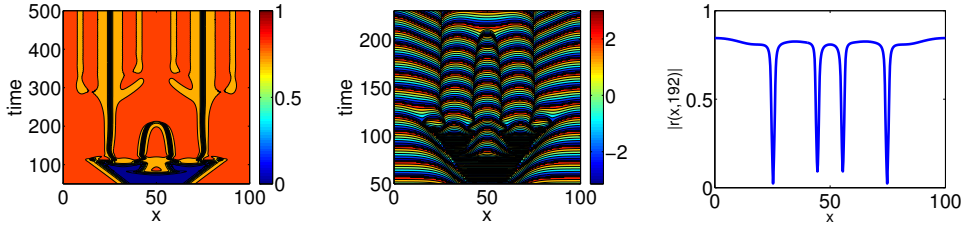

(a) $|r(x,t)|$ (b) $\theta(x,t)$ (c) $|r(x,192)|$

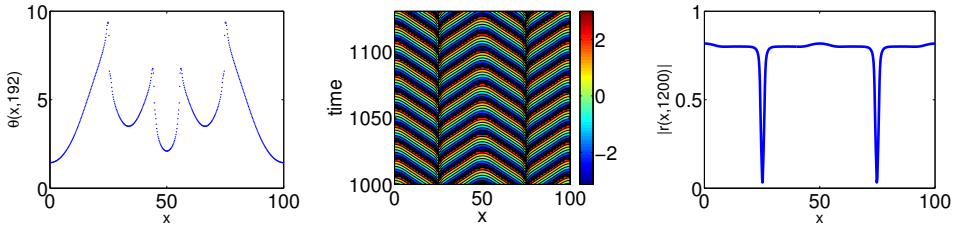

(d) $\theta(x,192)$ (e) $\theta(x,t)$ (f) $r(x,1200)$

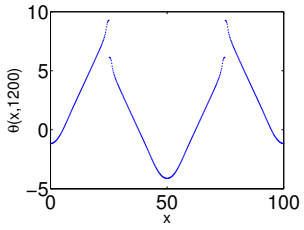

(g) $\theta(x,1200)$

Figure 3.5: Formation and dynamical evolution of hole patterns. (a) $|r(x,t)|$. (b-d) Close-up views of four hole patterns with two inner traveling holes. (e-g) Close-up views of two stationary hole patterns. ($\omega_0 = 5, T = 1, D = 100, k = 14.8$; initial condition: r is given by the homogeneous coherent state solutions for $0 \leq x \leq 41$ and $59 \leq x \leq 100$, and $r = 0$ otherwise; periodic boundary conditions are imposed).

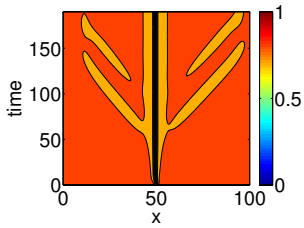

(a) $|r(x,t)|$

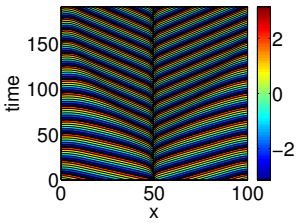

(b) $\theta(x,t)$

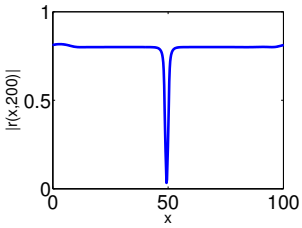

(c) $|r(x,200)|$

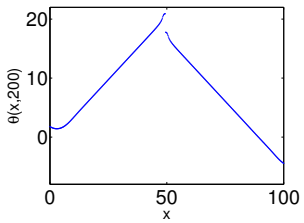

(d) $\theta(x,200)$

Figure 3.6: An example of the hole solution by collision of two plane wave solutions. The two waves meet at $x = 50$ with a π phase difference. ($\omega_0 = 5, T = 1, D = 100, k = 14.8$ and periodic boundary conditions). The initial condition corresponds to a discontinuous r given by a right traveling plane wave solution with $m = 3$ (where the wave number is $2m\pi/D$) for $0 \leq x \leq 50$ and a left traveling plane wave solution with $m = 4$ for $50 < x \leq 100$. Correspondingly, we observe from (d) that $[\theta(0,200) - \theta(100,200)] = 2\pi$.

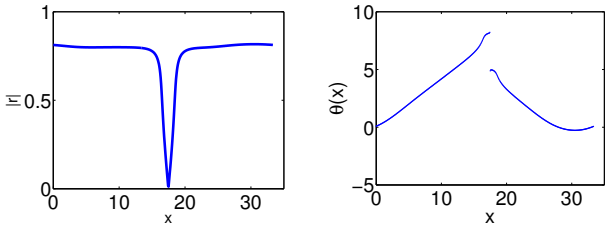

(a) $|r(x)|$ (b) $\theta(x)$

Figure 3.7: Finite width of (one-dimensional) hole core ($\omega_0 = 5, T = 1, D = 33.3, k = 14.8$).

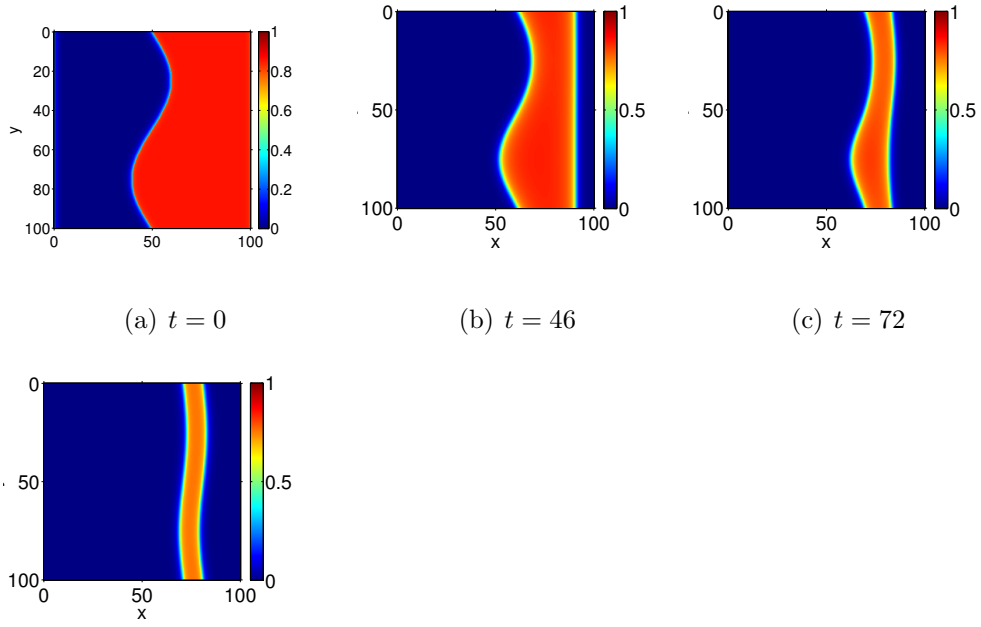

(a) $t = 0$ (b) $t = 46$ (c) $t = 72$

(d) $t = 216$

Figure 3.8: Time evolution of $|r(\mathbf{x}, t)|$ of a $d = 2$ configuration initialized with half of the region at the incoherent state and half at the coherent state divided by a wiggled boundary with $k = 14.4$ ($< k_c = 14.5$) ($\omega_0 = 5, T = 1, D = 100$; periodic boundary conditions are imposed).

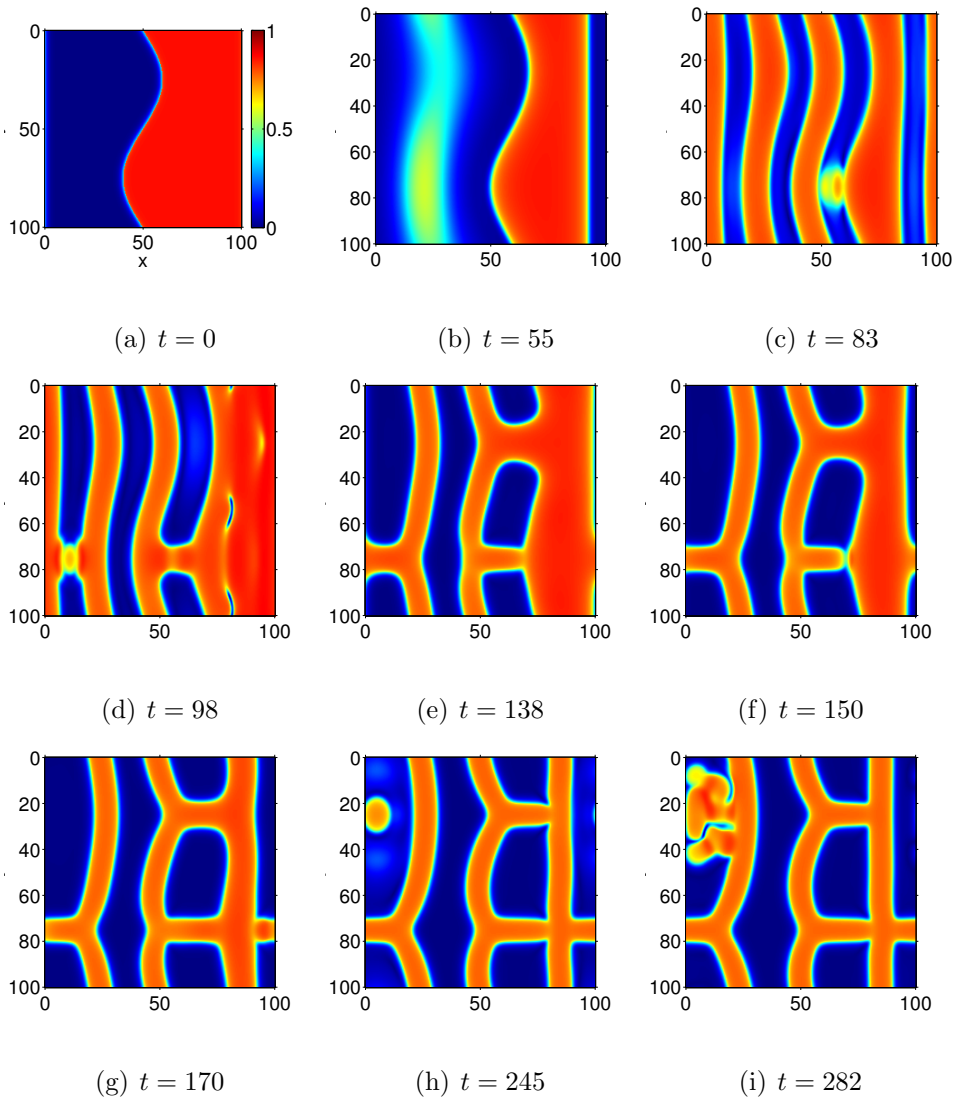

(a) $t = 0$ (b) $t = 55$ (c) $t = 83$

(d) $t = 98$ (e) $t = 138$ (f) $t = 150$

(g) $t = 170$ (h) $t = 245$ (i) $t = 282$

Figure 3.9: Time evolution of $|r(\mathbf{x}, t)|$ from an initial configuration (a) with half of the region at the incoherent state and half at the coherent state divided by a wiggled boundary with $k = 14.8$ ($> k_c = 14.5$). A comparison with Fig. 3.8 shows a much richer spatio-temporal dynamical pattern ($\omega_0 = 5, T = 1, D = 100$; periodic boundary conditions are imposed).

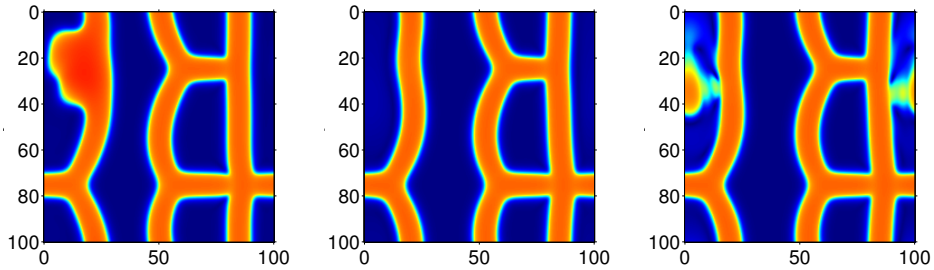

(j) $t = 303$ (k) $t = 400$ (l) $t = 431$

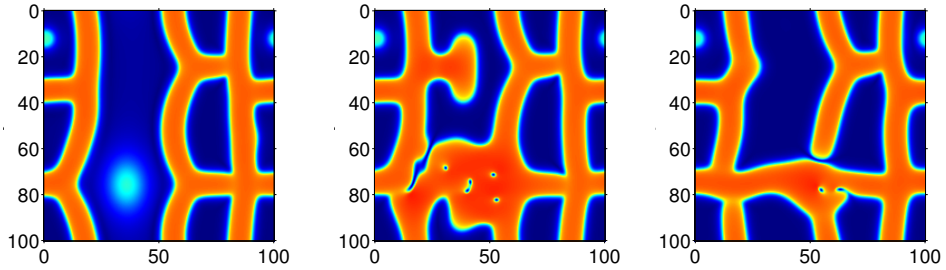

(m) $t = 561$ (n) $t = 611$ (o) $t = 669$

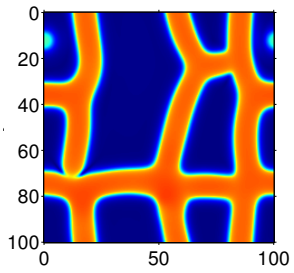

(p) $t = 700$

Figure 3.9: (Cont'd) Time evolution of $|r(\mathbf{x}, t)|$ from an initial configuration (a) with half of the region at the incoherent state and half at the coherent state divided by a wiggled boundary with $k = 14.8$ ($> k_c = 14.5$). A comparison with Fig. 3.8 shows a much richer spatio-temporal dynamical pattern ($\omega_0 = 5, T = 1, D = 100$; periodic boundary conditions are imposed).

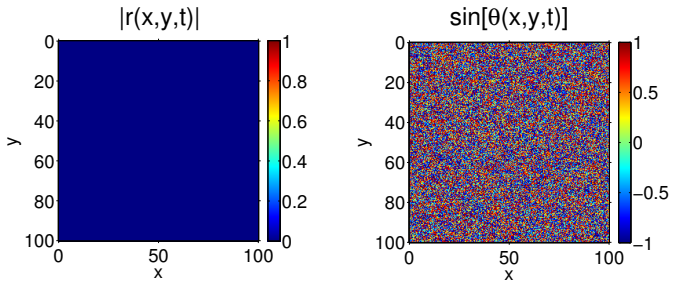

(a) $t = 0$ (b) $t = 0$

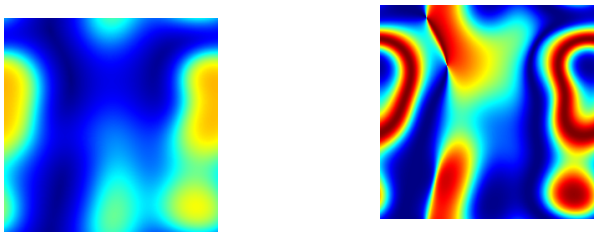

(c) $t = 40$ (d) $t = 40$

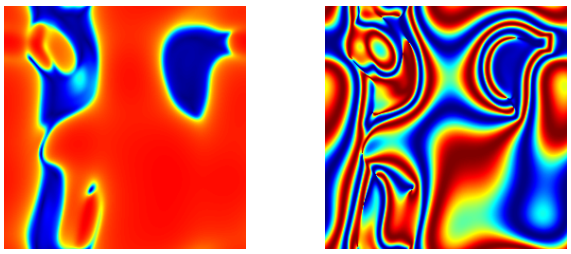

(e) $t = 57$ (f) $t = 57$

Figure 3.10: Time evolution of $|r(\mathbf{x}, t)|$ and $\sin[\theta(\mathbf{x}, t)]$ (where $r(\mathbf{x}, t) = |r(\mathbf{x}, t)| \exp[i\theta(\mathbf{x}, t)]$) from random initial condition, (a) and (b) ($\omega_0 = 5, T = 1, D = 100, k = 15.5$ ($> k_c = 14.5$); periodic boundary conditions are imposed).

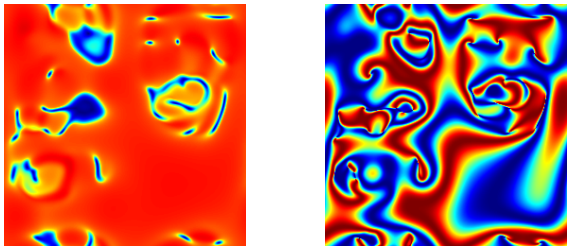

(g) $t = 87$ (h) $t = 87$

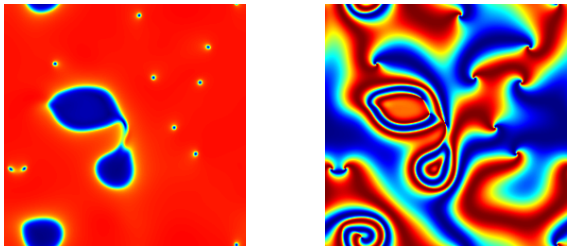

(i) $t = 139$ (j) $t = 139$

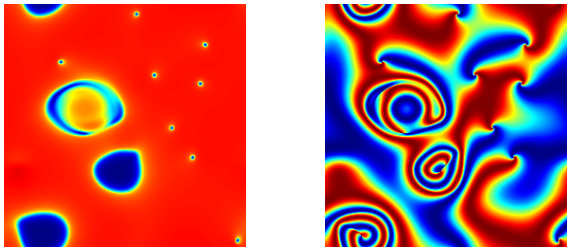

(k) $t = 153$ (l) $t = 153$

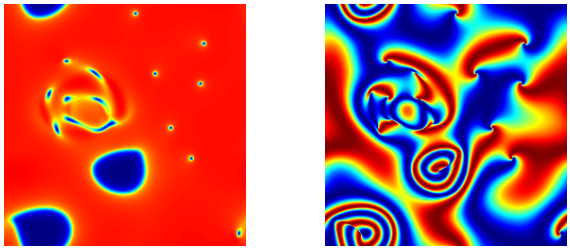

(m) $t = 161$ (n) $t = 161$

Figure 3.10: Cont'd

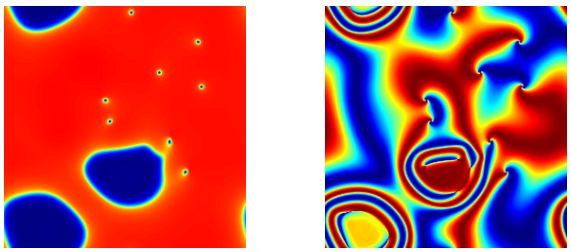

(o) $t = 195$ (p) $t = 195$

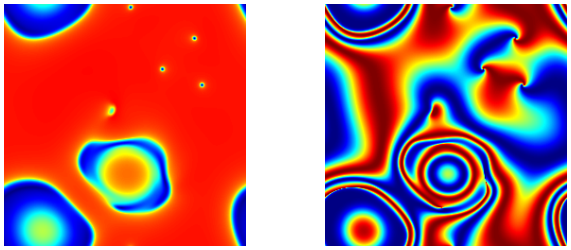

(q) $t = 217$ (r) $t = 217$

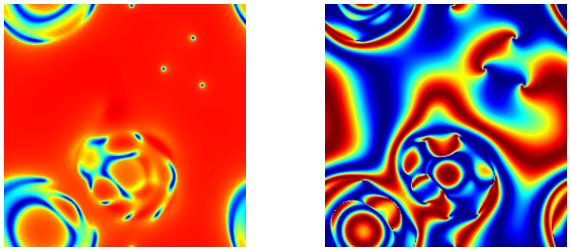

(s) $t = 225$ (t) $t = 225$

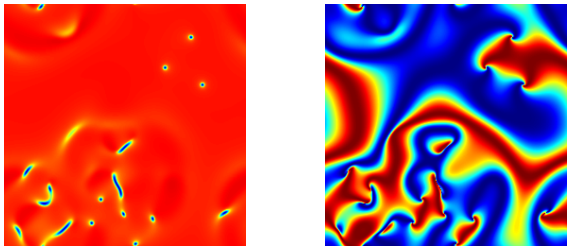

(u) $t = 238$ (v) $t = 238$

Figure 3.10: Cont'd

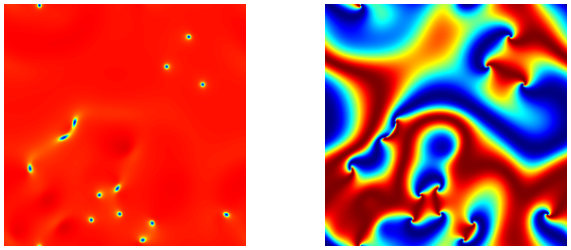

(w) $t = 250$ (x) $t = 250$

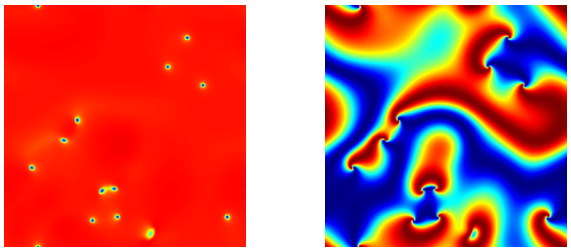

(y) $t = 259$ (z) $t = 259$

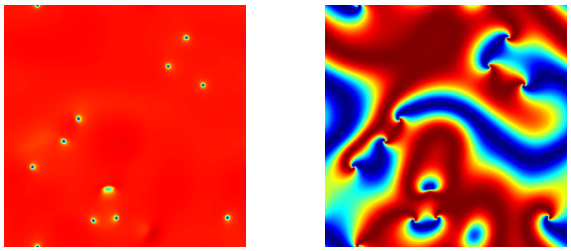

() $t = 263$ () $t = 263$

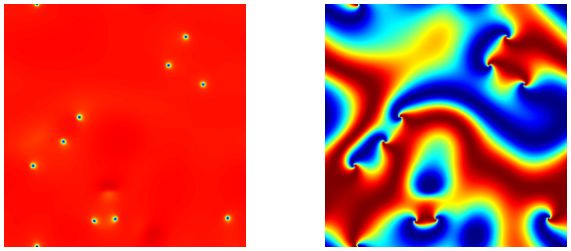

() $t = 267$ () $t = 267$

Figure 3.10: (Cont'd)

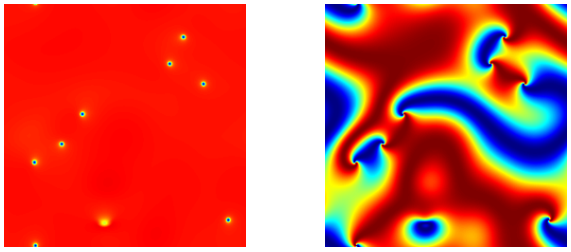

() $t = 281$ () $t = 281$

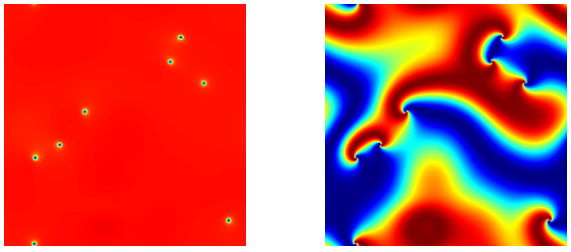

() $t = 293$ () $t = 293$

Figure 3.10: (Cont'd)Time evolution of $|r(\mathbf{x}, t)|$ and $\sin[\theta(\mathbf{x}, t)]$ (where $r(\mathbf{x}, t) = |r(\mathbf{x}, t)| \exp[i\theta(\mathbf{x}, t)]$) from random initial condition, (a) and (b) ($\omega_0 = 5, T = 1, D = 100, k = 15.5$ ($> k_c = 14.5$); periodic boundary conditions are imposed).

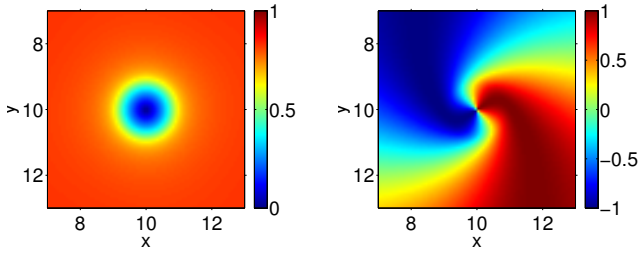

(a) $|r(\mathbf{x})|$ (b) $\sin(\theta(\mathbf{x}))$

Figure 3.11: Finite area of (two-dimensional) spiral cores ($\omega_0 = 5, T = 1, D = 20, k = 15$).

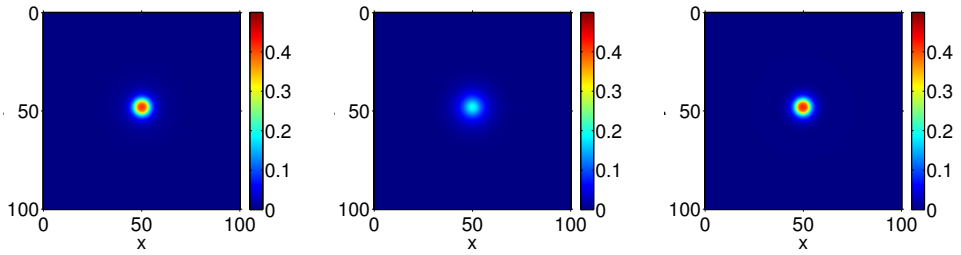

(a) $|r(\mathbf{x}, 129)|$ (b) $|r(\mathbf{x}, 148)|$ (c) $|r(\mathbf{x}, 158)|$

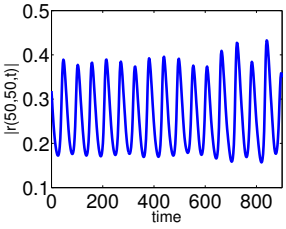

(d) $|r(50, 50, t)|$

Figure 3.12: Pulsating pattern: amplitude variation. Figures (a) to (c) show approximately one "period" of oscillation in $|r|$. Figure (d) shows the time variation of $|r|$ at the center of the pulse; compare with Fig. 3.13 for oscillations in phase ($\omega_0 = 5, T = 1, D = 100, k = 14.52$; periodic boundary conditions are imposed).

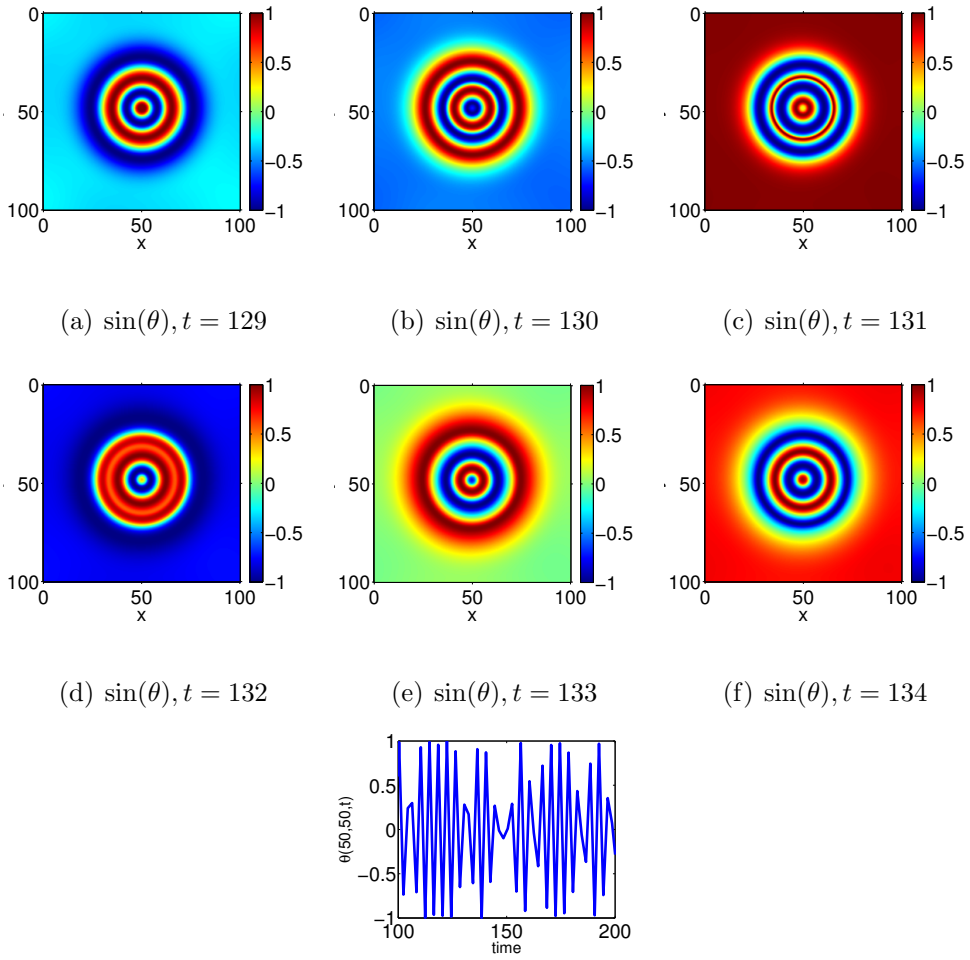

(a) $\sin(\theta), t = 129$ (b) $\sin(\theta), t = 130$ (c) $\sin(\theta), t = 131$

(d) $\sin(\theta), t = 132$ (e) $\sin(\theta), t = 133$ (f) $\sin(\theta), t = 134$

(g) $\sin(\theta(50, 50, t))$

Figure 3.13: Pulsating pattern: phase variation. Figures (a) to (f) show the rapid time variations of the phase. Figure (g) shows the time variation of $sin(\theta)$ at the center of the pulse (Parameters are as indicated in Fig. 3.12).

Chapter 4

Phase and amplitude dynamics in systems of coupled oscillators: growth heterogeneity, nonlinear frequency shifts, and locked states

4.1 Introduction

In the previous chapters, we focus our attention on modeling by the phase oscillator description. In the phase oscillator description the dynamical units are assumed to be oscillatory with fixed amplitude. Thus, the state of each individual unit can be specified solely by a phase angle θ, and the evolution of oscillator i is taken to be determined by its present state θ_i and by the states θ_j of the other oscillators ($j \neq i$). The simplest model of this type was originally put forward by Kuramoto in 1975 and has proven to be an extremely useful paradigm for understanding this general type of system [26, 27, 3, 64, 52]. In addition, the Kuramoto model has also

served as a basis for formulating related phase oscillator models appropriate to a wide variety of situations (e.g., see Refs. [53, 54, 55]). The basic question addressed by the Kuramoto model is the competition between the synchronizing effect of coupling and the desynchronizing effect of different natural frequencies of the individual oscillators. The principal result [26, 27, 3, 64, 52, 53, 54, 55] coming from the solution of the Kuramoto model is that, in the limit of a large number of oscillators, this competition is resolved by a transition, whereby there is a critical coupling strength below which the oscillations of individual oscillators occur with random phase and there is no macroscopic population-wide oscillation, while above which oscillators begin to develop phase coherence, and globally-averaged population-wide oscillation emerges.

A drawback of the phase oscillator description is that, by its definition, it excludes the effect of amplitude dynamics and the possible coupling of amplitude dynamics with phase dynamics. Another useful oscillator model incorporating amplitude dynamics is based on the normal form of an isolated system near a Hopf bifurcation,

$$\frac{dz}{dt} = (\alpha + i\omega)z - (\beta + i\gamma)|z|^2 z, \tag{4.1}$$

also referred to as a Landau-Stuart oscillator [57]. In (4.1) z is complex with $|z|$ and the angle of z representing the amplitude and phase of the oscillator. The real parameter α is the linear amplitude growth rate of the oscillations, with $\alpha > 0$ for growth (and $\alpha < 0$ for damping). The Hopf bifurcation occurs as α passes through

zero. The other real parameters ω, β, γ respectively characterize the small-amplitude natural frequency of the oscillator, and the finite amplitude nonlinear shifts of the small amplitude growth rate and frequency. The bifurcation is supercritical if $\beta > 0$ (the nonlinear term saturates growth) and subcritical (hysteretic) if $\beta < 0$ (the nonlinear term enhances growth). Here we will only deal with the supercritical case [in the subcritical case, if $\alpha > 0$, orbits typically go far from $z = 0$, thus invalidating the expansion resulting in (4.1)]. For $\alpha < 0$, Eq. (4.1) has as its stable solution $z = 0$. For $\alpha > 0$, $z = 0$ is unstable, and (4.1) results in an attracting limit cycle attractor,

$$z = \sqrt{\frac{\alpha}{\beta}} \exp\left[i \left(\omega - \frac{\gamma\alpha}{\beta} \right) t + \theta_0 \right], \tag{4.2}$$

which traces a circular orbit about the origin of the complex z-plane. In general, the normal form oscillator parameters $(\alpha, \omega, \beta, \gamma)$ derived from the physical system under study will depend on some set, $\mathbf{p} = (p^{(1)}, p^{(2)}, \cdots, p^{(n)})^T$, of physical parameters for that system. That is, $[\omega, \alpha, \beta, \gamma] = [\omega(\mathbf{p}), \alpha(\mathbf{p}), \beta(\mathbf{p}), \gamma(\mathbf{p})]$.

We are interested in the situation, also studied in Refs. [61, 16, 40, 37, 38, 11, 56], where many oscillators of the form of Eq. (4.1) are coupled together and where each such oscillator (indexed by a subscript $i = 1, 2, \cdots, N \gg 1$) may have a different parameter set. That is, if oscillator i has parameter set $\mathbf{p}_i$, then

$$[\omega_i, \alpha_i, \beta_i, \gamma_i] = [\omega(\mathbf{p}_i), \alpha(\mathbf{p}_i), \beta(\mathbf{p}_i), \gamma(\mathbf{p}_i)]. \tag{4.3}$$

If the value of $\mathbf{p}$ is regarded as assigned randomly from oscillator to oscillator ac-

cording to some probability distribution function (pdf), then that will induce a corresponding probability distribution function (pdf) $\hat{G}$ of the parameters $[\omega, \alpha, \beta, \gamma]$, such that

$$\hat{G}(\omega, \alpha, \beta, \gamma) d\omega d\alpha d\beta d\gamma \tag{4.4}$$

represents the fraction of oscillators with parameters $\omega, \alpha, \beta, \gamma$ in the range $\omega \in [\omega, \omega + d\omega]$, $\alpha \in [\alpha, \alpha + d\alpha]$, $\beta \in [\beta, \beta + d\beta]$, $\gamma \in [\gamma, \gamma + d\gamma]$, and applicable in the limit $N \to \infty$, where N is the number of oscillators.

Considering this general problem, one would like to know how the system behavior depends on the distribution function $\hat{G}(\omega, \alpha, \beta, \gamma)$. However, as $\hat{G}$ is a distribution in the four variables $\omega, \alpha, \beta, \gamma$, this is clearly too big a problem to address in full generality. Here we will pursue a more modest program. In particular, the situation we treat is motivated by the experimental work in Ref. [67], which suggests the following questions: (i) what is the effect of spread in α allowing the simultaneous presence of dead ($\alpha < 0$) and active ($\alpha > 0$) oscillators in the uncoupled state, and (ii) what is the effect of a nonlinear frequency shift γ (for simplicity, we treat the oscillators as all having the same γ), and iii) how we can understand a certain type of simple nonlinear behavior often observed in these systems when the coupling strength between oscillators is large?

4.2 Formulation, background and outline

We assume β and γ are the same for all oscillators, $\beta_i = \bar{\beta}$ and $\gamma_i = \bar{\gamma}$. Furthermore, we scale $\bar{\beta}$ to one by a proper normalization of z_i ($z_i \to z_i/\sqrt{\bar{\beta}}$). Thus

$$\hat{G}(\omega, \alpha, \beta, \gamma) = G(\omega, \alpha)\delta(\beta - 1)\delta(\gamma - \bar{\gamma}). \tag{4.5}$$

If ω and α are uncorrelated in their variation from oscillator to oscillator, then G is of the form

$$G(\omega, \alpha) = g(\omega)h(\alpha). \tag{4.6}$$

In what follows we assume that Eq. (4.6) holds [1], and that $g(\omega)$ is symmetric and monotonically decreasing with respect to its maximum value, which we can take to be located at $\omega = 0$ (if the maximum of $g(\omega)$ occurred at some non-zero value, $\omega = \bar{\omega}$, then the location of the maximum can be shifted to zero by the change of variables $z = z'e^{i\bar{\omega}t}$, $\omega' = \omega - \bar{\omega}$).

For (4.1) with $\beta_i = 1$, $\gamma_i = \bar{\gamma}$ and (4.6) specifying our ensemble of uncoupled oscillators, we now proceed to globally couple these ensemble members through a mean field, $\langle z \rangle$,

$$\frac{dz_i}{dt} = (\alpha_i + i\omega_i)z_i - (1 + i\bar{\gamma})|z_i|^2 z_i + \Gamma\langle z \rangle, \tag{4.7a}$$

$$\langle z \rangle = \frac{1}{N}\sum_{j=1}^{N} z_j, \tag{4.7b}$$

[1] In general, however, we note that ω and α can be expected to have correlations; e.g., even if the physical parameter vector $\mathbf{p}$ has dimension $n \geq 2$ and the variation of components are uncorrelated, we can still expect that the particular functional dependences, Eq. (4.3), of the oscillator parameters on the physical parameters will induce correlations between ω and α.

where the parameter Γ measures the strength of the coupling and is assumed real and positive, $\Gamma \geq 0$. Letting angle brackets denote averaging over all oscillators, we will sometimes refer to $\langle z \rangle$ as the "order parameter" because whether or not there is global collective behavior for $N \to \infty$ corresponds to whether $|\langle z \rangle| > 0$ or $\langle z \rangle = 0$. See Refs. [61, 16, 40, 37, 38, 11, 56] for previous related work on large coupled systems of Landau-Stuart equations. Note that in many of these works [61, 16, 40, 37, 38] the coupling term is written as $K(\langle z \rangle - z_i)$ in place of $\Gamma \langle z \rangle$. This choice is simply related to ours by the transformation $\alpha_i = \hat{\alpha}_i - K$, $\Gamma = K$. We prefer the parametrization in Eq. (4.7) because one of our principal motivations will be experiments [67] where it can be plausibly argued that quantities analogous to Γ and the average value of α_i (denoted $\bar{\alpha}$) can be varied essentially independently. In addition, in Refs. [61, 16, 40, 37, 38] it was considered that $\hat{\alpha}_i$ was the same positive constant for all i, $\hat{\alpha}_i = \hat{\alpha}$, and furthermore that $\bar{\gamma} = 0$. Parameter and time normalizations were then chosen to transform $\hat{\alpha}$ to 1, yielding, in place of (4.7)

$$\frac{dz_i}{dt} = (i\omega_i + 1 - |z_i|^2)z_i + K(\langle z \rangle - z_i). \tag{4.8}$$

We, however, will be interested in the effect of a spread in α_i with the possibility of the simultaneous occurrence of positive and negative α_i for different i, and also in the effects of nonlinear frequency shift $\bar{\gamma} \neq 0$.

A principal motivation for this study is the recent paper, Ref. [67], which describes experiments in which many ($\sim 10^4/cm^3$) specially designed small porous particles are continuously and rapidly mixed in a catalyst-free Belousov-Zhabotinsky

reaction mixture. The catalyst for the reaction is immobilized on the small porous particles, each of which can potentially serve as an effective chemical oscillator. Oscillations in the chemical states of the particles are visualized as the color of the particles oscillates between red and blue. The particle density serves as a parameter analogous to our coupling constant Γ, while regulation of the stirring rate effectively provides a control analogous to control of the mean oscillator growth rate,

$$\bar{\alpha} = \int \alpha h(\alpha) d\alpha. \tag{4.9}$$

Because the process by which the particles are prepared is not perfect, it is expected that there will be substantial spread in their parameters, and in particular in ω and α. These spreads are of particular interest because: (i) spread of oscillator frequencies is the essential feature leading to the transition from incoherently oscillating units to macroscopic oscillation in the Kuramoto model, and (ii) the parameter α determines whether individual particles, when uncoupled, oscillate ($\alpha > 0$) or do not oscillate ($\alpha < 0$). In the case $\alpha < 0$ the attractor for Eq. (4.1) is the fixed point $z = 0$, often referred to as "oscillator death". With reference to point (ii), because of the spread in α, in some range of stirring rates, we can expect a situation like that shown schematically in Fig. 4.1, which depicts an uncoupled oscillator growth rate pdf $h(\alpha)$ yielding substantial fractions of the particles in the oscillating and dead states. As $\bar{\alpha}$ increases from very negative values, $(-\bar{\alpha}) \gg \delta\alpha$) (analogous to low stirring rates in the experiment), to very positive values, $\bar{\alpha} \gg \delta\alpha$ (analogous to high stirring rates), there is a continuous transition from predominantly dead to

predominantly oscillatory dynamics of the uncoupled oscillators. Another notable feature of these experiments is that the collective coherent frequency of oscillation exhibits a marked dependence on the oscillation amplitude through its dependence on the density of the porous particles at fixed stirring rate (e.g., the third panels in Fig. 2(a) and 2(b) of Ref. [67]). This is a strong indication that the nonlinear frequency shift $\bar{\gamma}$ plays a significant role. It is notable that Ref. [67] developed a set of chemical rate equations that, when solved numerically, yield good agreement with the experiments. While this is a singular achievement, we are interested in obtaining additional understanding of the processes involved and in determining its genericity. To the extent that qualitative behavior of our Landau-Stuart model mimics behavior observed in the particular experiment in Ref. [67], the typicality of the observed phenomena is strongly implied. Furthermore, if the above agreement holds, then any analytical results obtained for the Landau-Stuart model may lead to further understanding of these experimental phenomena. Thus it is our desire to employ the generic coupled Landau-Stuart model, Eqs. (4.7), to explore and understand the nature of the interplay between frequency spread, growth rate spread and nonlinear frequency shift. In this connection, it is worth noting that our work may be applicable to other experiments. Indeed, as described in Ref. [67], the chemical experiment was, at least partly, intended to mimic observed oscillator quorum-sensing in yeast populations [13, 41]. In addition, the basic stability analysis technique used here (Sect. 4.3) is similar to that originally introduced in Refs. [37] and [38] can also be applied to other amplitude / phase oscillator systems, such as the laser system considered in Ref. [73].

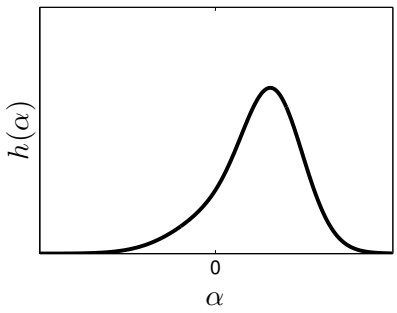

Figure 4.1: Schematics of $h(\alpha)$.

We now give a brief review of the most important papers [61, 16, 40, 37, 38, 11, 56] related to our work. References [61, 16, 40, 37, 38] considered Eq. (4.8) (all oscillators have identical α_i and $\gamma_i = 0$) and examined the behavior as a function of the coupling constant K and the spread σ in the oscillator frequencies. Shiino and Frankowicz [61] by a combination of numerical experiments and analysis obtain an approximate $K - \sigma$ plane phase diagram. References [16, 40] examine the transition between "amplitude death" [2] (i.e., $z_i = 0$ for all oscillators) and collective oscillation, explicitly obtaining analytical results for the boundary in $K - \sigma$ space separating death and collective oscillation.

Matthews et al. [37, 38], in addition to presenting an extensive numerical exploration, also develop an analytical technique for handling the transition to globally coherent oscillation from phase-incoherent individual oscillation with $|z_i| > 0$ (as in

[2] In addition to the situation of many coupled Landau-Stuart equations, oscillator death occurs very generally for many types of coupled oscillator situations, including coupling between only a few oscillators (e.g., two). As an example of one of the many references on this topic, we note the recent paper, Ref. [66], and references therein.

the Kuramoto transition [27, 3, 64, 52, 53, 54]); thus this work was the first to include analysis of the effect of amplitude dynamics on this type of transition. In addition, another important result of Refs. [37, 38] was the numerical discovery that near the boundary in parameter space where the transition to collective behavior occurs, this collective behavior can be rather complex, including period doubling cascades, chaos, quasiperiodicity and hysteresis. Further, sufficiently far above the boundary it was found that steady oscillatory behavior prevails (as in the Kuramoto model).

Reference [11] introduces a situation that the authors call "aging" in which there are two populations, each described by an equation of the form of (4.7) (with $\alpha_i = \hat{\alpha} - K$ and $\Gamma = K$); the "old" population has $\hat{\alpha}_i = -\hat{\alpha}_o < 0$ (corresponding to amplitude death at $K = 0$), and the "young" population has $\hat{\alpha}_i = \hat{\alpha}_y > 0$; ω_i was taken to be the same constant Ω for all old and young oscillators (see also [56] which allows distinct old and young natural frequencies, $\omega_i = \Omega_o$ and Ω_y); and behavior was investigated as a function of the ratio of the populations of old relative to young. In the set up of Refs. [11, 56], due to the homogeneity of frequencies, the transition problem reduces to the analysis of two coupled Landau-Stuart equations.

The rest of this chapter is organized as follows. Section 4.3 derives the characteristic equation governing linear stability of perturbations from the $\langle z \rangle = 0$ state. Section 4.4 evaluates the characteristic equation for the case of a Lorentzian frequency distribution, $g(\omega) = [\pi(1 + \omega^2)]^{-1}$. Section 4.5 evaluates the effect of spread in α on linear stability in the case of Lorentzian $g(\omega)$ and no nonlinear frequency shift ($\bar{\gamma} = 0$). Section 4.6 evaluates the effect of nonlinear frequency shift ($\bar{\gamma} \neq 0$) on

stability in the case of Lorentzian $g(\omega)$ and no spread in α. Section 4.7 uses the example of a flat-top frequency distribution, $g(\omega) = U(1-|\omega|)/2$ (where $U(\bullet)$ denotes the unit step function) to show that the qualitative behavior found in Secs. 4.5 and 4.6 is insensitive to the form of $g(\omega)$. Section 4.8 discusses behavior above the instability threshold for cases when there is no spread in the nonlinear parameters β and γ of (4.1) (as in Eq. (4.7)). Section 4.9 studies stability of the corresponding nonlinear solutions in the limit of large coupling, $\Gamma/\Gamma_c \to \infty$, where Γ_c denotes the critical value of Γ at which the $\langle z \rangle = 0$ state becomes unstable. A primary issue addressed in Secs. 4.8 and 4.9 is the explanation of why a purely oscillatory state with constant amplitude (referred to as the "locked state") can always be observed for the macroscopic solutions as Γ/Γ_c is increased. Conclusions and further discussions are given in Sec. 4.10.

4.3 Linear stability of the $\langle z \rangle = 0$ state

We consider Eqs. (4.7) in the limit $N \to \infty$. In this case, there is a solution corresponding to zero value of the order parameter $\langle z \rangle$. For $\langle z \rangle = 0$, Eq. (4.7a) has the solutions

$$z_i = 0 \ \text{ for } \ \alpha_i < 0, \tag{4.10a}$$

$$z_i = \sqrt{\alpha_i}\exp\{i[(\omega_i - \bar{\gamma}\alpha_i)t + \theta_{0i}]\} \ \text{ for } \ \alpha_i > 0. \tag{4.10b}$$

We express the order parameter $\langle z \rangle$ as

$$\langle z \rangle = \langle z \rangle_- + \langle z \rangle_+, \tag{4.11a}$$

$$\langle z \rangle_- = \frac{1}{N} \sum_{i,\alpha_i<0} z_i, \tag{4.11b}$$

$$\langle z \rangle_+ = \frac{1}{N} \sum_{i,\alpha_i>0} z_i, \tag{4.11c}$$

That is, $\langle z \rangle_-$ and $\langle z \rangle_+$ denote the contribution to the order parameter from oscillators with $\alpha_i < 0$ and $\alpha_i > 0$, respectively. Note that (4.10a) implies $\langle z \rangle_- = 0$, while (4.10b) implies $\langle z \rangle_+ = 0$ if $N \to \infty$ and the angles θ_{0i} are uniformly distributed in $[0, 2\pi]$. Thus, by (4.11a), we see that $\langle z \rangle = 0$ is indeed a self-consistent solution of the system (4.7) for $N \to \infty$. We now ask whether this solution is stable to small perturbations. If it is not, then the state $\langle z \rangle = 0$ will not persist, and global collective behavior will result. We denote the perturbation of the order parameter by

$$\langle \delta z \rangle = \langle \delta z \rangle_- + \langle \delta z \rangle_+, \tag{4.12a}$$

$$\langle \delta z \rangle_\pm = \frac{1}{N} \sum_{i,\alpha_i \gtrless 0} \delta z_i, \tag{4.12b}$$

where δz_i is a perturbation from the unperturbed orbit dynamics given by Eqs. (4.10).

Calculation of $\langle \delta z \rangle_-$. Considering oscillator i for which $\alpha_i < 0$, and perturbing Eq. (4.7a) about $z_i = 0$, we obtain the linearized equation,

$$\frac{d\delta z_i}{dt} = (\alpha_i + i\omega_i)\delta z_i + \Gamma\langle\delta z\rangle. \tag{4.13}$$

Assuming exponential time dependence of the orbit perturbations, $\delta z_i \sim \exp(st)$, Eq. (4.13) yields

$$\delta z_i = \frac{\Gamma\langle\delta z\rangle}{(s + |\alpha_i| - i\omega)} \text{ for } \alpha_i < 0. \tag{4.14}$$

Thus

$$\langle\delta z\rangle_- = \Gamma\langle\delta z\rangle \int_{-\infty}^{\infty}\int_{-\infty}^{0} \frac{g(\omega)h(\alpha)}{(s + |\alpha| - i\omega)} d\alpha d\omega, \tag{4.15}$$

where for $N \to \infty$ we have replaced the sum over i in (4.11b) by integration over ω and α weighted by the pdf's $g(\omega)$ and $h(\alpha)$ [Eq. (4.6)]. Note that the α integration in (4.15) runs from $\alpha = -\infty$ to $\alpha = 0$ and thus includes only those oscillators for which $\alpha < 0$.

Formulation for calculating $\langle\delta z\rangle_+$. We begin by re-expressing Eq. (4.7a) in polar form, $z_i = \rho_i \exp(i\theta_i)$ where $\rho_i(t)$ and $\theta_i(t)$ are real,

$$\frac{d\rho_i}{dt} = \alpha_i\rho_i - \rho_i^3 + \Gamma Re\{e^{-i\theta}\langle z\rangle\}, \tag{4.16a}$$

$$\frac{d\theta_i}{dt} = \omega_i - \bar{\gamma}\rho_i^2 + \frac{\Gamma}{\rho_i} Im\{e^{-i\theta}\langle z\rangle\}, \tag{4.16b}$$

$$\langle z\rangle = \langle\rho e^{i\theta}\rangle. \tag{4.16c}$$

We now introduce a pdf for the state variables (ρ, θ) and parameters (ω, α) which we denote by

$$f(\rho, \theta, \omega, \alpha, t).$$

Thus

$$\int_0^{2\pi} \int_0^{\infty} f d\rho d\theta = g(\omega)h(\alpha).$$

By conservation of the number of oscillators and Eqs. (4.16), f satisfies the following continuity equation,

$$\begin{aligned} &\frac{\partial f}{\partial t} + \frac{\partial}{\partial \rho}\left\{\left[\alpha\rho - \rho^3 + \frac{\Gamma}{2}\left(e^{-i\theta}\langle z\rangle + e^{i\theta}\langle z\rangle^*\right)\right] f\right\} \\ &\quad + \frac{\partial}{\partial \theta}\left\{\left[\omega - \bar{\gamma}\rho^2 + \frac{\Gamma}{2i\rho}\left(e^{-i\theta}\langle z\rangle - e^{i\theta}\langle z\rangle^*\right)\right] f\right\} = 0, \end{aligned} \tag{4.17}$$

where

$$\langle z\rangle = \iiint \rho e^{i\theta} f d\rho d\theta d\omega d\alpha. \tag{4.18}$$

For $\alpha > 0$ the time independent incoherent ($\langle z\rangle_+ \equiv 0$) solution of (4.17) and (4.18) is

$$f_0 = \frac{g(\omega)h(\alpha)}{2\pi}\delta(\rho - \sqrt{\alpha}). \tag{4.19}$$

We now introduce a perturbation to the solution (4.19),

$$f = f_0 + e^{st - i\theta}\delta f + \{O.P.T.\}, \tag{4.20}$$

where $\{O.P.T.\}$ denotes "other perturbation terms" whose θ variation is proportional to $\exp(in\theta)$ with $n \neq -1$. These other terms do not contribute to $\langle z\rangle_+$ [see Eq. (4.18)] and so turn out to be of no consequence to what follows. Inserting (4.20) and (4.19) into (4.17) we obtain for $\alpha > 0$

$$(s - i\omega + i\bar{\gamma}\rho^2)\delta f + \frac{\partial}{\partial\rho}\left[(\alpha - \rho^2)\rho\delta f\right] = \frac{\Gamma\langle\delta z\rangle g(\omega)h(\alpha)}{4\pi}\left\{\frac{\delta(\rho - \sqrt{\alpha})}{\sqrt{\alpha}} - \delta'(\rho - \sqrt{\alpha})\right\}, \tag{4.21}$$

where

$$\delta'(\rho - \sqrt{\alpha}) = \frac{d}{d\rho}\delta(\rho - \sqrt{\alpha}).$$

Calculation of $\langle\delta z\rangle_+$. We now solve (4.21) for δf. To do this we assume a solution of the form

$$\delta f = \frac{\Gamma\langle\delta z\rangle g(\omega)h(\alpha)}{4\pi}[c_1(\omega, s)\delta(\rho - \sqrt{\alpha}) + c_2(\omega, s)\delta'(\rho - \sqrt{\alpha})], \tag{4.22}$$

and substitute this assumed form into (4.21). Using the delta function identities

$$F(\rho)\delta(\rho - \sqrt{\alpha}) = F(\sqrt{\alpha})\delta(\rho - \sqrt{\alpha}),$$
$$F(\rho)\delta'(\rho - \sqrt{\alpha}) = F(\sqrt{\alpha})\delta'(\rho - \sqrt{\alpha}) - F'(\sqrt{\alpha})\delta(\rho - \sqrt{\alpha}),$$

(where the second of these identities follows from differentiating the first), Eq. (4.21) yields

$$T_1 + T_2 = \frac{1}{\sqrt{\alpha}}\delta - \delta' \tag{4.23}$$

where $\delta = \delta(\rho - \sqrt{\alpha})$, $\delta' = \delta'(\rho - \sqrt{\alpha})$, T_1 results from the first term on the left hand side of (4.21),

$$
\begin{aligned}
T_1 &= (s - i\omega \quad + i\bar{\gamma}\rho^2)(c_1\delta + c_2\delta') \\
&= (s - i\omega \quad + i\bar{\gamma}\alpha)(c_1\delta + c_2\delta') - 2i\bar{\gamma}\sqrt{\alpha}c_2\delta,
\end{aligned}
$$

and T_2 results from the second term on the left hand side of (4.21),

$$
T_2 = \frac{\partial}{\partial\rho}\{(\alpha - \rho^2)\rho(c_1\delta + c_2\delta')\} = 2\alpha c_2\delta'.
$$

Separately equating coefficients of δ and δ' on the two sides of (4.23), we obtain two linear equations for the coefficients c_1 and c_2. Solution of these equations yields

$$
\begin{aligned}
c_1 &= \frac{1}{\sqrt{\alpha}}\frac{s - i\omega + 2\alpha - i\bar{\gamma}\alpha}{s - i\omega + 2\alpha + i\bar{\gamma}\alpha} \cdot \frac{1}{s - i\omega + i\bar{\gamma}\alpha}, \\
c_2 &= -\frac{1}{s - i\omega + i\bar{\gamma}\alpha + 2\alpha}.
\end{aligned}
$$

Insertion of (4.22) with these expressions for c_1 and c_2 into (4.18) then yields $\langle\delta z\rangle_+$,

$$
\begin{aligned}
\langle\delta z\rangle_+ =& \Gamma\langle\delta z\rangle \int_{-\infty}^{+\infty} d\omega g(\omega) \\
& \left\{\int_0^{+\infty} \frac{(s - i\omega + \alpha)h(\alpha)}{[s - i\omega + 2\alpha + i\bar{\gamma}\alpha][s - i\omega + i\bar{\gamma}\alpha]} d\alpha\right\}.
\end{aligned}
\tag{4.24}
$$

Note that the α integration in (4.24) is only over positive α (i.e., the integration runs from $\alpha = 0$ to $\alpha = \infty$.)

Equation determining s. Inserting (4.15) and (4.24) into (4.12a) we obtain,

$$
\begin{aligned}
\Gamma^{-1} = & \int_{-\infty}^{\infty}\int_0^{+\infty} \frac{(s - i\omega + \alpha)g(\omega)h(\alpha)d\alpha d\omega}{[s - i\omega + 2\alpha + i\bar{\gamma}\alpha][s - i\omega + i\bar{\gamma}\alpha]} \\
& + \int_{-\infty}^{\infty}\int_{-\infty}^{0} \frac{g(\omega)h(\alpha)d\alpha d\omega}{s + |\alpha| - i\omega} \equiv D(s).
\end{aligned}
\tag{4.25}
$$

By causality, this expression for the dispersion function $D(s)$, as well as our previous results, Eqs. (4.15) and (4.24), for $\langle \delta z \rangle_-$ and $\langle \delta z \rangle_+$, apply if the ω-integration poles are in the lower half ω-plane. This condition is satisfied for both of the integrals in (4.25) and all values of α if $Re(s) > 0$. Since we are interested in the occurrence of instability, and instability corresponds to $Re(s) > 0$, the form giving $D(s)$ by (4.25) is sufficient for our purposes ($D(s)$ for $Re(s) \leq 0$ can be obtained by analytic continuation, from the $Re(s) > 0$ result).

4.4 Lorentzian Frequency Distribution

As discussed in Sec. 4.1, and as we will verify by the example in Sec. 4.7, we believe that different monotonically decreasing, continuous frequency distribution functions $g(\omega)$ often yield similar qualitative behaviors (but see Ref. [51]), and we, therefore, specialize here to one such $g(\omega)$ that allows easy analytic evaluation of the integrals over ω, namely, the case of Lorentzian $g(\omega)$,

$$g(\omega) = \frac{1}{\pi} \frac{1}{\omega^2 + 1} = \frac{1}{2\pi i} \left\{ \frac{1}{\omega - i} - \frac{1}{\omega + i} \right\}, \tag{4.26}$$

where we have adopted a normalization of t, Γ and α so that the half-width of $g(\omega)$ is one ($g(0) = 2g(1)$). Since $Re(s) > 0$, the only ω-pole of the integrands in (4.25) that is located in $Im(\omega) \geq 0$ is the one at $\omega = i$ [see Eq. (4.26)]. In addition, the magnitudes of the integrands behave like $|\omega|^{-3}$ for large $|\omega|$. Thus, we can deform the ω-integration path by shifting it upward into the complex ω-plane, letting $Im(\omega)$ along the path approach $+\infty$. The integration then yields the residue of the pole

at $\omega = i$,

$$D(s) = \int_0^{+\infty} \frac{(s+1+\alpha)h(\alpha)d\alpha}{[s+1+2\alpha+i\bar{\gamma}\alpha][s+1+i\bar{\gamma}\alpha]} + \int_{-\infty}^{0} \frac{h(\alpha)d\alpha}{s+|\alpha|+1}. \tag{4.27}$$

In Sec. 4.5 we investigate conditions under which Eq. (4.27) predicts instability (i.e., existence of a solution to $D(s) = \Gamma^{-1}$ with $Re(s) > 0$).

4.5 Condition for Instability: The effect of a spread in the growth rates in α

In this section, we consider the case where there is no nonlinear frequency shift (i.e., $\bar{\gamma} = 0$), with $g(\omega)$ being Lorentzian. Using a generalization of the technique in Ref. [40] (see proof of their Theorem 2), it can be shown that the solution of $D(s) = 1/\Gamma$ is real. Thus, as we pass from stability to instability, s goes through $s = 0$. This results in the following general condition for instability,

$$\Gamma > \frac{1}{D(0)}, \tag{4.28}$$

and (4.27) and (4.28) imply that instability occurs when Γ exceeds the critical value Γ_c given by

$$\Gamma_c = \left\{ \int_0^{\infty} \frac{\alpha+1}{2\alpha+1} h(\alpha)d\alpha + \int_{-\infty}^{0} \frac{1}{1-\alpha} h(\alpha) \right\}^{-1}. \tag{4.29}$$

As a simple reference case, we first consider (4.29) when there is no dispersion in α,

$$h(\alpha) = \delta(\alpha - \bar{\alpha})$$

in which case we obtain

$$\Gamma_c = \begin{cases} (2\bar{\alpha}+1)/(\bar{\alpha}+1), & \text{for } \bar{\alpha} \geq 0, \\ 1+|\bar{\alpha}|, & \text{for } \bar{\alpha} \leq 0. \end{cases} \tag{4.30}$$

The resulting phase diagram is given by the black line in Fig. 4.2. This result (with the different parametrization used in Eq. (4.8)) has been previously obtained in Refs. [37, 38]. Note that $\Gamma_c \to 2$ as $\bar{\alpha} \to +\infty$. The value $\Gamma_c = 2$ is the critical coupling value that applies for the Kuramoto model with a Lorentzian frequency pdf, Eq. (4.26). The applicability of the Kuramoto result for large $\bar{\alpha}$ can be understood from Eq. (4.16a) with Γ neglected, $d\rho/dt = \bar{\alpha}\rho - \rho^3$, which when linearized about the incoherent equilibrium value, $\rho = \sqrt{\bar{\alpha}}$, yields $d\delta\rho/dt = -2\bar{\alpha}\delta\rho$. Thus perturbations from $\rho = \sqrt{\bar{\alpha}}$ relax at the exponential rate $2\bar{\alpha}$, and, for large $\bar{\alpha}$, this rate becomes much faster than the other relevant time scale, namely, the spread in ω (which we have normalized to 1). Hence, for $\bar{\alpha} \gg 1$, the oscillator amplitude is essentially frozen, and the Kuramoto oscillator description is valid. As shown in Fig. 4.2 and Eq. (4.30), when $\bar{\alpha} \gg 1$ does not hold, the effect of amplitude dynamics is to reduce Γ_c (for $\bar{\alpha} \geq 0$) from the Kuramoto value with the reduction increasing to a factor of 2 as $\bar{\alpha} \to 0^+$ ($\Gamma_c = 2$ at $\bar{\alpha} \to +\infty$ in comparison with $\Gamma_c = 1$ at $\bar{\alpha} = 0$). An additional interesting point is that comparison of the black line in Fig. 4.2 with the results for the phase diagram in the case of Belousov-Zhabotinsky system of Ref. [67] (see discussion in Sect. 4.1) shows a striking qualitative similarity between the two (e.g., see Fig. 3 of Ref. [67]).

Referring to Eq. (4.30) and Fig. 4.2, we see that there is a sharp transition in behavior as $\bar{\alpha}$ crosses $\bar{\alpha} = 0$. In particular, the $\langle z \rangle = 0$ state for $\bar{\alpha} < 0$ results

from the fact that $z_i = 0$ for all oscillators, while for $\bar{\alpha} > 0$ all oscillators have $|z_i| = \sqrt{\bar{\alpha}} > 0$ and $\langle z \rangle = 0$ results from incoherence of the individual oscillator phases. This sharp transition in behavior is reflected by the discontinuity of the derivative, $d\Gamma_c/d\bar{\alpha}$, at $\bar{\alpha} = 0$. The sharp nature of the transition at $\bar{\alpha} = 0$ is, however, a nonphysical artifact of the assumption of no dispersion in the individual oscillator growth / damping rates used in obtaining (4.30). In typical physical situations, such as the experiment in Ref. [67] (see discussion in Sect. 4.2), dispersion in α is to be expected (Fig. 4.1). To simply illustrate its effect we consider the example where $h(\alpha)$ is uniform within some range $\delta\alpha$ about an average value $\bar{\alpha}$,

$$h(\alpha) = (2\delta\alpha)^{-1} U(\delta\alpha - |\alpha - \bar{\alpha}|), \tag{4.31}$$

where $U(x)$ denotes the unit step function; $U(x) = 1$ for $x \geq 0$ and $U(x) = 0$ for $x < 0$. Using (4.31) in (4.29), we get for $\bar{\alpha} > \delta\alpha$,

$$\Gamma_c^{-1} = \frac{1}{2\delta\alpha} \left[\delta\alpha + \frac{1}{4} \ln \left(\frac{\bar{\alpha} + \delta\alpha + 1/2}{\bar{\alpha} - \delta\alpha + 1/2} \right) \right]; \tag{4.32}$$

for $\bar{\alpha} < -\delta\alpha$,

$$\Gamma_c^{-1} = \frac{1}{2\delta\alpha} \ln \left(\frac{1 - \bar{\alpha} + \delta\alpha}{1 - \bar{\alpha} - \delta\alpha} \right); \tag{4.33}$$

and for $|\bar{\alpha}| < \delta\alpha$,

$$\Gamma_c^{-1} = \frac{1}{2\delta\alpha} \left[\frac{\bar{\alpha} + \delta\alpha}{2} + \ln(1 - \bar{\alpha} + \delta\alpha) + \frac{1}{4} \ln(1 + 2\bar{\alpha} + 2\delta\alpha) \right]. \tag{4.34}$$

As the dispersion in α, $\delta\alpha$, approaches zero, (4.31) becomes a delta function, and Eqs. (4.32)-(4.34) reduce to (4.30). The other two lines in Fig. 4.2 show the phase diagram from Eqs. (4.32)-(4.34) for two more values of $\delta\alpha$. For $\delta\alpha > 0$ the

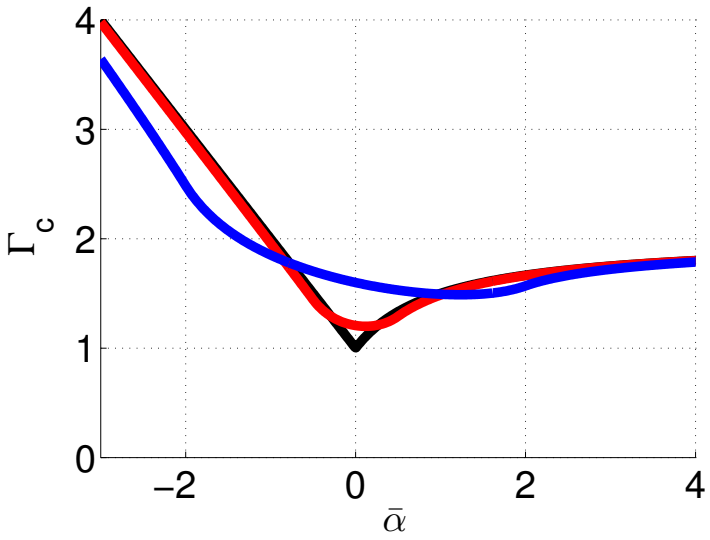

Figure 4.2: The effect of dispersion in α ($\bar{\gamma} = 0$) with a Lorentzian $g(\omega)$. Stability/Instability regions of $\Gamma - \bar{\alpha}$ space for several different values of spread $\delta\alpha$ in the linear growth parameter α with mean $\bar{\alpha}$ [Legend: Black line ($\delta\alpha = 0$), red line ($\delta\alpha = 0.5$), blue line ($\delta\alpha = 2$)].

discontinuity in $d\Gamma_c/d\bar{\alpha}$ (which occurs for $\delta\alpha = 0$ at $\bar{\alpha} = 0$) is removed by dispersion in α, and the sharp transition that occurs at $\bar{\alpha} = 0$ (black line in Fig. 4.2) is now smoothed out [3]. Further, it is also noticed that the minimum of Γ_c rises and shifts from $\bar{\alpha} = 0$ when $\delta\alpha = 0$ to $\bar{\alpha} > 0$ when $\delta\alpha > 0$.

[3]Equation (4.29) [together with a transformation of the form of the interaction term to that of Eq. (4.8)] can also be used to generalize previous work of Ref. [11] on the "aging transition" to include dispersion of the natural frequencies.

4.6 The effect of a nonlinear frequency shift

We now address the effect of nonlinear frequency shift, $\bar{\gamma} \neq 0$, and we consider the simple case of no dispersion in α, $h(\alpha) = \delta(\alpha - \bar{\alpha})$ again for the case of Lorentzian $g(\omega)$. We note from Eq. (4.7), if the distribution of ω_i values is symmetric, then positive and negative values of $\bar{\gamma}$ are equivalent ($z_i \to z_i^*$). Thus, we consider $\bar{\gamma} > 0$ only. As is evident from Eq. (4.27), $\bar{\gamma}$ has no effect on the linear theory for $\bar{\alpha} < 0$, and, consequently, the result for Γ_c given by Eq. (4.30) still applies for $\bar{\alpha} \leq 0$. For $\bar{\alpha} > 0$, however, the effect of a nonlinear frequency shift can be substantial. Equation (4.27) for $h(\alpha) = \delta(\alpha - \bar{\alpha})$, $\bar{\alpha} > 0$ gives

$$\Gamma^{-1} = D(s) = \frac{s + 1 + \bar{\alpha}}{(s + 1 + 2\bar{\alpha} + i\bar{\gamma}\bar{\alpha})(s + 1 + i\bar{\gamma}\bar{\alpha})}, \tag{4.35}$$

which yields a quadratic equation for s, solution of which can be used to obtain stability boundary curves in $\Gamma - \bar{\alpha}$ space. At the transition point, $Re(s)$ goes through zero. Substituting $s = i\Omega$ into Eq. (4.35) and separating the real and imaginary parts, Γ_c and Ω are then given by the solution of the following pair of equations

$$1 - \Omega^2 + 2\bar{\alpha}(1 - \bar{\gamma}\Omega) - \bar{\alpha}^2\bar{\gamma}^2 = \Gamma_c(1 + \bar{\alpha}), \tag{4.36a}$$

$$2(1 + \bar{\alpha})(\Omega + \bar{\alpha}\bar{\gamma}) = \Gamma_c\Omega. \tag{4.36b}$$

When $\bar{\gamma} = 0$ (note $\Omega = 0$ for this case), the solution for the critical coupling strength of (4.36) is given by

$$\Gamma_{c0} = \frac{1 + 2\bar{\alpha}}{1 + \bar{\alpha}}, \tag{4.37}$$

by which (4.36a) can be rearranged to give

$$\Gamma_c = \Gamma_{c0} - \frac{(\Omega + \bar{\alpha}\bar{\gamma})^2}{1 + \bar{\alpha}}, \tag{4.38}$$

which shows that the effect of $\bar{\gamma}$ is always to decrease Γ_c. Figure 4.3 shows the values of Γ_c as a function of $\bar{\alpha}$ for several different values of $\bar{\gamma}$ ($\bar{\gamma} = 0$ plotted in black, $\bar{\gamma} = 2$ plotted in red, and $\bar{\gamma} = 4$ plotted in blue). By solving for Ω in (4.36b) and substituting it back in (4.36a), we obtain

$$\Gamma_c = \Gamma_{c0} - \frac{1}{1 + \bar{\alpha}} \left[\frac{\bar{\alpha}\bar{\gamma}\Gamma_c}{\Gamma_c - 2(1 + \bar{\alpha})} \right]^2. \tag{4.39}$$

Equation (4.39) shows that $\Gamma_c \to 2$ as $\bar{\alpha} \to +\infty$. As seen in Fig. 4.3, increasing $\bar{\gamma}$ eventually moves the minimum of Γ_c below one and shifts the location of the minimum into $\bar{\alpha} > 0$.

4.7 The effect of the frequency distribution function

In Secs. 4.5 and 4.6 we consider the effect of a spread in α and of a nonlinear frequency shift for the illustrative case of a Lorentzian distribution function of the oscillator natural frequencies, Eq. (4.26). We now ask how might these results be altered if a different frequency distribution were used. We note that the Lorentzian decays rather slowly for large ω, $g(\omega) \sim \omega^{-2}$. Thus to test dependence on the form of $g(\omega)$, we will examine another distribution function which is very different from the Lorentzian, in that it has a sharp cutoff to $g(\omega) = 0$ as ω increases. In particular, we will consider a "flat-top" distribution, that is uniform in $-1 \leq \omega \leq 1$ and zero otherwise,

$$g(\omega) = \frac{1}{2} U(1 - |\omega|), \tag{4.40}$$

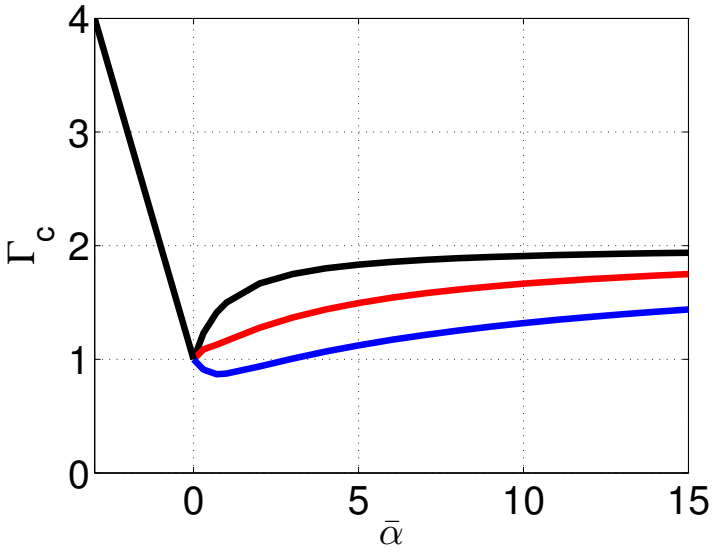

Figure 4.3: Stability / Instability regions of $\Gamma - \bar{\alpha}$ space for several different values of the nonlinear frequency shift parameter $\bar{\gamma}$ [Legend: Black line ($\bar{\gamma} = 0$), red line ($\bar{\gamma} = 2$), blue line ($\bar{\gamma} = 4$)]. Notice that the three lines coincide when $\bar{\alpha} < 0$.

where $U(x)$ is the unit step function. In spite the qualitatively different large $|\omega|$ behaviors of the Lorentzian and the flat-top $g(\omega)$ distributions, we will find that the resulting stability conditions show qualitatively similar behaviors.

The calculation of Γ_c with $g(\omega)$ given by (4.40) is done by using (4.25) (see Appendix A). In Fig. 4.4 we show the dependence of Γ_c on $\bar{\alpha}$ for several different values of $\delta\alpha$, where $h(\alpha)$ is given by (4.31) and $\bar{\gamma} = 0$ for all oscillators. A comparison between Fig. 4.4 and Fig. 4.2 reveals remarkably similar dependence, apart from a difference in the vertical scale due to different functional dependence of $g(\omega)$ [4]. Next, we consider the dependence of Γ_c on $\bar{\gamma}$ when $h(\alpha) = \delta(\alpha - \bar{\alpha})$ with $g(\omega)$ given by (4.40). Figure 4.5 shows the dependence of Γ_c on $\bar{\alpha}$ for several different values of $\bar{\gamma}$. The black line shows the result when $\bar{\gamma} = 0$, which is the same black line in Fig. 4.4. The other two lines are obtained by numerically solving (A.7) when $\bar{\gamma} \neq 0$. In comparison with Fig. 4.3, we see similar dependence in that, as $\bar{\gamma}$ increases, Γ_c decreases.

4.8 Nonlinear phenomena above the instability threshold with finite α-spread and nonlinear frequency shift

In the previous sections, we calculated the critical coupling strength Γ_c marking the onset of instability of the quiescent state ($\langle z \rangle = 0$). Above the critical value Γ_c, we find that Landau-Stuart oscillator networks exhibit a rich variety of collective behavior. We now briefly first review past work on the nonlinear behavior found

[4] It can be shown that when $h(\alpha) = \delta(\alpha - 1)$, $\Gamma_c^{-1} = \pi g(0)$ for any general unimodal frequency distribution $g(\omega)$ symmetric about $\omega = 0$ (see Ref. [38]).

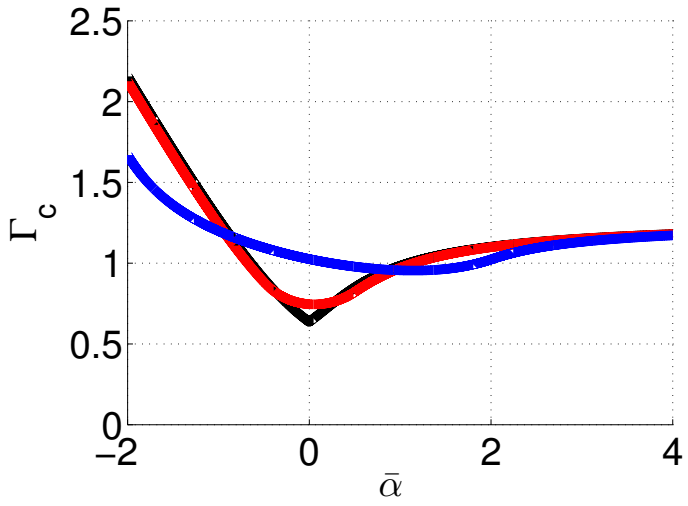

Figure 4.4: The effect of dispersion in α with a uniformly distributed $g(\omega)$, Eq. (4.40). Stability/Instability regions of $\Gamma - \bar{\alpha}$ space for several different values of spread $\delta\alpha$ in the linear growth paratmeter α with mean $\bar{\alpha}$ [Legend: Black line ($\delta\alpha = 0$), red line ($\delta\alpha = 0.5$), blue line ($\delta\alpha = 2.0$)].

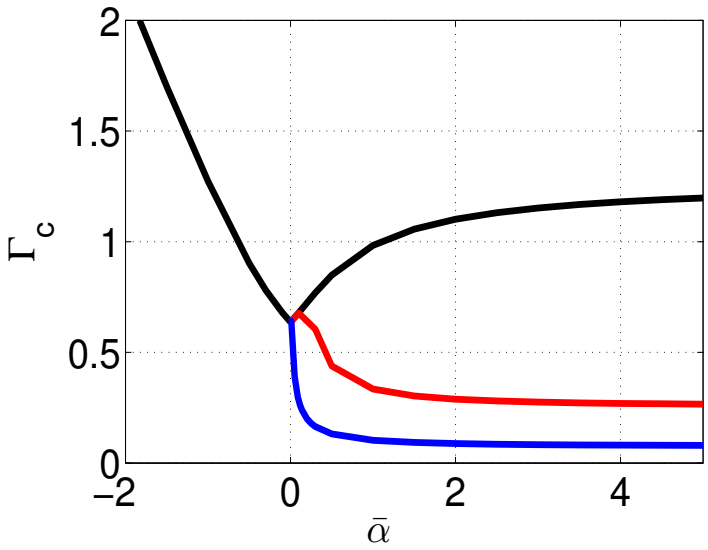

Figure 4.5: Stability / Instability regions of $\Gamma - \bar{\alpha}$ space for several different values of the nonlinear frequency shift parameter $\bar{\gamma}$ [Legend: Black line ($\bar{\gamma} = 0$), red line ($\bar{\gamma} = 2$), blue line ($\bar{\gamma} = 4$)]. Notice that the three lines coincide when $\bar{\alpha} < 0$.

above the instability threshold.

Matthews et al. [38] study nonlinear collective behaviors in the special case when $\alpha_j = 1$ and $\gamma_j = 0$ for all oscillators ($j = 1, 2, \cdots N$), and $g(\omega)$ takes on several different functional forms. An important observation in that paper is that the system behavior can be quite complicated for a range of Γ not too far above Γ_c, e.g., there are period doubling cascades to chaos, large amplitude oscillations, quasiperiodicity, hysteretic behavior close to the boundaries between different macroscopic states, etc. However, when Γ is sufficiently far from Γ_c, the system is found to settle into a simple steady oscillatory state, $\langle z \rangle = constant \times \exp(i\Omega t)$ for some constant Ω. We refer to this as a "locked state".

When the nonlinear frequency shift parameter $\bar{\gamma}$ is nonzero [20, 47, 48, 49], the system can exhibit an additional type of complicated coherent behavior. For example, Refs. [20, 47, 48, 49, 12] study systems closely related to Eq. (4.7), but with homogeneous parameters. An important feature found in those references is the tendency for the system to form clusters (a "cluster" in the above references is defined as a group of oscillators which behave identically). Further, depending on parameter values and on initial conditions, the systems can form cluster states of varying sizes. In Refs. [47] and [48], the authors also find chaotic behavior.

Despite the complications noted above, we emphasize the important result that in all these cases, the system can always settle into a simple locked state when Γ is sufficiently large. Furthermore, in our own simulations which (unlike previous work) include spreads in α, and ω, and simultaneously allow $\beta_j = \bar{\beta} \neq 0$ and $\gamma_j = \bar{\gamma} \neq 0$, it is again always found that, as Γ is increased, there is always a locked state solution

that the system can settle into. As an example, Fig. 4.6 shows snapshots of the long-time asymptotic distributions of the oscillator $z-$values obtained from numerical simulations of Eq. (4.7) with $g(\omega)$ given by (4.40), $N = 50000$, $h(\alpha)$ given by (4.31), $\bar{\alpha} = 0.5$, $\delta\alpha = 1.0$, $\bar{\gamma} = 0.5$ (corresponding to $\Gamma_c = 0.89$), for successively larger values of Γ/Γ_c, all of which are large enough that a locked state is achieved (Fig. 4.6(a): $\Gamma/\Gamma_c = 2$, Fig. 4.6(b): $\Gamma/\Gamma_c = 10$, Fig. 4.6(c): $\Gamma/\Gamma_c = 100$). Note that, as appropriate for a locked state, as time increases, these snapshots rotate uniformly about the origin at a fixed angular rate Ω.

We see in Fig. 4.6(a) that the distribution has finite spreads in both the magnitude and phase of z. Examination of the solution shows that oscillators with smaller (larger) natural frequencies ω tend to occur on the clockwise (counterclockwise) side of the distribution, while larger (smaller) α tend to occur at larger (smaller) $|z|$ for fixed argument of z. Previous works (e.g., [38]) did not consider a distribution of α and consequently did not find a spread in $|z|$ at constant argument of z (i.e., the oscillators are distributed along a curve in the complex z-plane). Comparing Figs. 4.6(a), 4.6(b) and 4.6(c), we see that the spread in $z/|\langle z\rangle|$ becomes smaller and smaller as Γ/Γ_c increases. In fact, we argue in Sec. 4.9 below that this spread goes to zero as $\Gamma/\Gamma_c \to \infty$ (note the greatly magnified scale for Fig. 4.6(c)).

Figure 4.7 illustrates an example of the occurrence and evolution of a non-locked dynamical attractor at lower Γ/Γ_c with other parameters the same as those in Fig. 4.6. In particular, Fig. 4.7 shows $|\langle z\rangle|$ (top panel) and $\mathrm{Re}\langle z\rangle$ (bottom panel) versus time, after the system has settled into an attractor for $\Gamma/\Gamma_c = 1.07$. (Note that for a locked state, $|\langle z\rangle|$ is constant, and $\mathrm{Re}\langle z\rangle$ varies sinusoidally in time.)

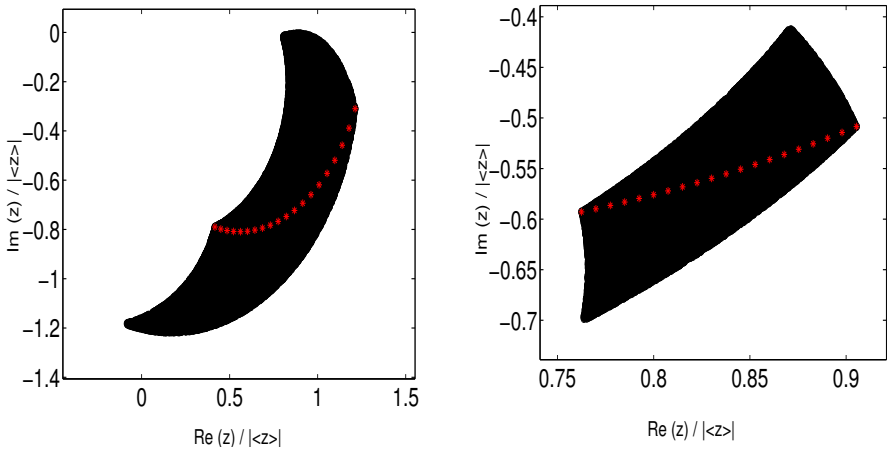

(a) $\Gamma/\Gamma_c = 2$ (b) $\Gamma/\Gamma_c = 10$

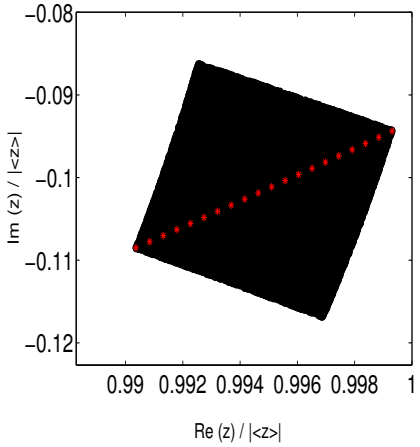

(c) $\Gamma/\Gamma_c = 100$

Figure 4.6: Locations of 50000 oscillators (black) in the locked states with different Γ/Γ_c. Twenty oscillators (red cross) of parameter values evenly spaced simultaneously in $(\alpha, \omega) \in [-0.5, 1.5] \times [-1, 1]$ are highlighted, i.e., the oscillator with $(\alpha, \omega) = (-0.5, -1)$ is located at the minimum radius position, and the oscillator with $(\alpha, \omega) = (1.5, 1)$ is located at the maximum radius position, and other oscillators of intermediate parameter values evenly distributed in between ($N = 50000$, $\bar{\alpha} = 0.5$, $\delta\alpha = 1.0$, $\bar{\gamma} = 0.5$; random initial conditions).

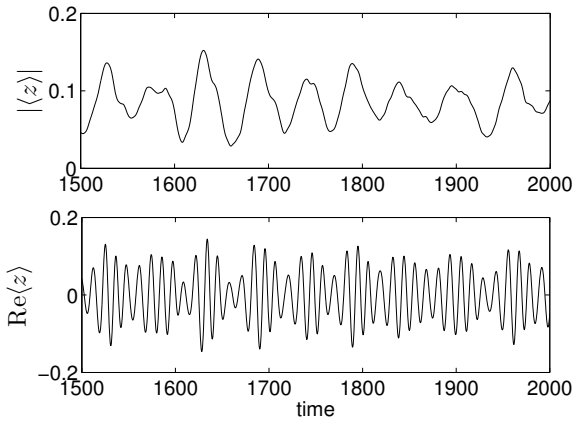

Figure 4.7: Time evolution of $|\langle z \rangle|$ (top panel) and $\mathrm{Re}\langle z \rangle$ (bottom panel) for a system of $500,000$ oscillators (Parameters: $\bar{\alpha} = 0.5$, $\delta\alpha = 1.0$, $\bar{\gamma} = 0.5$, $\Gamma/\Gamma_c = 1.07$; random initial conditions.)

4.9 Large coupled Landau-Stuart oscillator networks in the strong coupling limit

An important exception to the observation of locked states at sufficiently large Γ has been noted by Montbrió and Pazó [44] who studied the situation where there was a spread in the nonlinear frequency shift. They showed that, in that case, locked states do not necessarily exist for large Γ, and that other behaviors can occur. In our further works [32, 33] we will further investigate the subtle effects of constant nonlinearity parameters $\bar{\gamma}$ and $\bar{\beta}$, and effects due to spreads in the γ_j and β_j distributions without employing the weak coupling approximation of Montbrió and Pazó [44]. In what follows we, as in all other previous references (except for [44]) consider the case where there is no spread in the nonlinear coefficients ($\gamma_j = \bar{\gamma}$

and $\beta_j = \bar{\beta}$ for all j), and we ask why the locked state applies for large enough Γ.

In order to analytically show that a locked state must result for homogeneous nonlinearity parameters $\bar{\gamma}$ and $\bar{\beta}$ at sufficiently large Γ/Γ_c, we now consider very large Γ/Γ_c approximated by taking the limit $\Gamma/\Gamma_c \to \infty$. In particular, using this limit, we will show the existence of a locked state and we will demonstrate that it is stable.

When $\Gamma \gg \alpha_j, \omega_j$ for all j, system (4.7) reduces to

$$\frac{dz_j}{dt} = -(1 + i\bar{\gamma})|z_j|^2 z_j + \Gamma\langle z\rangle. \tag{4.41}$$

Here we have assumed that $|z_j| \gg 1$ in the $\Gamma \to \infty$ limit. This will be subsequently verified. Alternatively, if the ω_j are uniform, $\omega_j = \omega$, and $\Gamma \gg \alpha_j$, even if $\Gamma \gg \omega$ does not apply, we can still obtain Eq.(4.41) via elimination of ω through the transformation $z_j \to z_j e^{i\omega t}$. Thus, in this limit, the dynamics is determined by the coupling to other oscillators and the nonlinear characteristics of the individual oscillators, rather than by the linear properties of the individual oscillators. This is consistent with our numerical tests in Fig. 4.6, which suggests that as $\Gamma/\Gamma_c \to \infty$, the distribution of oscillators approaches that of a system of homogeneous parameter values, with the effects of spreads due to α and ω going away (see Fig. 4.6(c)). We now divide Eq.(4.41) by Γ, and redefine variables as

$$\hat{z}_j = \frac{z_j}{\sqrt{\Gamma}}, \tag{4.42a}$$

$$\hat{t} = \Gamma t. \tag{4.42b}$$

Thus, each term in Eq. (4.41) scales as $\Gamma^{3/2}$ justifying the neglect of the other terms in Eq. (4.7). Equations (4.41) become

$$\frac{d\hat{z}_j}{d\hat{t}} = -(1+i\bar{\gamma})|\hat{z}_j|^2\hat{z}_j + \frac{1}{N}\sum_{k=1}^{N}\hat{z}_k, \tag{4.43}$$

Taking the locked state ansatz $\hat{z}_j = \rho(\hat{t})\exp\{i[\theta(\hat{t})+\phi_j)]\}$ and considering the case when all the ϕ_j are the same, gives

$$\frac{d\rho}{d\hat{t}} = \rho(1-\rho^2), \tag{4.44a}$$

$$\frac{d\theta}{d\hat{t}} = -\gamma\rho^2, \tag{4.44b}$$

where, without loss of generality we set $\phi_j = 0$ for all j. This yields the asymptotic solution,

$$\hat{z_0}(\hat{t}) = e^{-i\gamma\hat{t}}. \tag{4.45}$$

To analyze the stability of (4.45), we perturb $\hat{z}_0$ to $\hat{z}_0 + e^{-i\gamma\hat{t}}\delta\hat{z}_j$. From (4.43), the dynamics of $\delta\hat{z}_j$ is governed by

$$\frac{d}{d\hat{t}}\delta\hat{z}_j = (-1-i\gamma)\left(\delta\hat{z}_j + \delta\hat{z}_j^*\right) - \delta\hat{z}_j + \frac{1}{N}\sum_k \delta\hat{z}_k. \tag{4.46}$$

where * denotes complex conjugation. Similarly, we have

$$\frac{d}{d\hat{t}}\delta\hat{z}_j^* = (-1+i\gamma)\left(\delta\hat{z}_j + \delta\hat{z}_j^*\right) - \delta\hat{z}_j^* + \frac{1}{N}\sum_k \delta\hat{z}_k^*. \tag{4.47}$$

Equations (4.46) and (4.47) can be regarded as two independent equations for $\delta\hat{z}_j$ and $\delta\hat{z}_j^*$ respectively. To study the stability properties of $\delta\hat{z}_j$ and $\delta\hat{z}_j^*$, consider $\delta\hat{z}_j \sim \delta\hat{Z}_j(s)e^{s\hat{t}}$ and $\delta\hat{z}_j^* \sim \delta\hat{Z}_j^*(s)e^{s\hat{t}}$, for which Eqs. (4.46) and (4.47) give

$$(s+2+i\gamma)\,\delta\hat{Z}_j + (1+i\gamma)\,\delta\hat{Z}_j^* - \langle\delta\hat{Z}\rangle = 0, \tag{4.48a}$$

$$(s+2-i\gamma)\,\delta\hat{Z}_j^* + (1-i\gamma)\,\delta\hat{Z}_j - \langle\delta\hat{Z}^*\rangle = 0, \tag{4.48b}$$

where $\langle\delta\hat{Z}\rangle = N^{-1}\sum_k \delta\hat{Z}_k$, $\langle\delta\hat{Z}^*\rangle = N^{-1}\sum_k \delta\hat{Z}_k^*$. Summing over j we obtain

$$\Upsilon \begin{bmatrix} \langle\delta\hat{Z}\rangle \\ \\ \langle\delta\hat{Z}^*\rangle \end{bmatrix} = 0, \tag{4.49}$$

where

$$\Upsilon \equiv \begin{bmatrix} (s+1+i\gamma) & (1+i\gamma) \\ \\ (1-i\gamma) & (s+1-i\gamma) \end{bmatrix}. \tag{4.50}$$

Equation (4.49) implies that either (i) $\det\Upsilon = 0$, or (ii)$\langle\delta\hat{Z}\rangle = \langle\delta\hat{Z}^*\rangle = 0$. Possibility (i) gives $s(s+2) = 0$, yielding $s = 0$ and $s = -2$. Physically, the neutrally stable root, $s = 0$, corresponds to a uniform, rigid rotation of the phases of all the $\hat{Z}_j$. If possibility (ii) applies, Eqs. (4.48a) and (4.48b) become

$$\Psi \begin{bmatrix} \delta\hat{Z}_j \\ \\ \delta\hat{Z}_j^* \end{bmatrix} = 0, \tag{4.51}$$

where

$$\Psi \equiv \begin{bmatrix} (s+2+i\gamma) & (1+i\gamma) \\ \\ (1-i\gamma) & (s+2-i\gamma) \end{bmatrix}. \tag{4.52}$$

Since $\det\Psi = (s+1)(s+3)$, we obtain two additional roots $s = -1$ and $s = -3$. Because the allowed perturbations in case (ii) are restricted to lie in the $2(N-1)$ dimensional space specified by the two constraints, $\langle\delta\hat{Z}\rangle = 0$ and $\langle\delta\hat{Z}^*\rangle = 0$, the

multiplicity of each of the roots $s = -1$ and $s = -3$ is $N - 1$. Since there is no root with $Re(s) > 0$, the equilibrium is stable.

4.10 Conclusions

In this chapter we have studied some properties of large all-to-all coupled Landau-Stuart oscillator networks which have both amplitude and phase degrees of freedom. In the first half of the chapter, motivated by experiments reported in Ref. [67], we studied stability of the incoherent state ($\langle z \rangle = 0$) and determined the stability / instability boundary for different cases. First, we studied networks with spread in the distribution of the linear amplitude growth parameter α, but with no nonlinear frequency shift contribution, i.e., $\gamma = 0$ for all oscillators. Second, we studied networks with no spread in the distribution α, but with a constant nonlinear frequency shift parameter $\bar{\gamma}$ for all oscillators. After establishing a mathematical framework to determine the stability / instability boundary, we characterized the changes in the stability / instability boundary that these modifications cause. First, we found that a spread $\delta\alpha$ in the distribution of α smoothes out the sharp transition at $\bar{\alpha} = 0$ if $\delta\alpha = 0$. Second, spread in α causes the minimum of Γ_c to shift away from $\bar{\alpha} = 0$ to $\bar{\alpha} > 0$ when $\delta\alpha > 0$. Third, increase of the nonlinear frequency shift parameter $\bar{\gamma}$ monotonically lowers Γ_c.

Similar to large networks of phase oscillators of the Kuramoto type, large networks of Landau-Stuart oscillators can synchronize into a locked state exhibiting steady constant amplitude sinusoidal motion when the coupling strength is large enough. In order to better understand this behavior, we studied locked states of Eq.

(4.7) with homogeneous nonlinearity parameters in the limit $\Gamma/\Gamma_c \to \infty$. We found that as $\Gamma/\Gamma_c \to \infty$, Eq. (4.7) reduces to Eq. (4.43), which depends only on coupling among oscillators through the constant nonlinear characteristics. Furthermore, we showed that such locked states are stable. And this answers the question why a locked state can always be observed for the system studied.

Appendix A

Theoretical values of the critical coupling strength with a uniformly distributed $g(\omega)$

In this appendix we summarize the theoretical results of the critical coupling strength Γ_c when $g(\omega)$ is given by the uniform distribution

$$g(\omega) = \frac{1}{2}U(1 - |\omega|), \tag{A.1}$$

First, we determine Γ_c when there is no spread in $h(\alpha)$, i.e., $h(\alpha) = \delta(\alpha - \bar{\alpha})$, and $\gamma = 0$ for all oscillators. When $\bar{\alpha} > 0$, we have

$$\Gamma_c^{-1} = \frac{\pi}{4} + \frac{1}{2}\tan^{-1}\left(\frac{1}{2\bar{\alpha}}\right); \tag{A.2}$$

similarly, when $\bar{\alpha} < 0$, we have

$$\Gamma_c^{-1} = \tan^{-1}\left(\frac{1}{|\bar{\alpha}|}\right). \tag{A.3}$$

For the cases when there is spread in $h(\alpha)$, we assume the same model $h(\alpha) = (2\delta\alpha)^{-1}U(\delta\alpha - |\alpha - \bar{\alpha}|)$. By denoting $\bar{\alpha}_+ = \bar{\alpha} + \delta\alpha$ and $\bar{\alpha}_- = \bar{\alpha} - \delta\alpha$, we have for

$\bar{\alpha} > \delta\alpha$,

$$\Gamma_c^{-1} = \frac{\pi}{4} + \frac{1}{4\delta\alpha}\left[\bar{\alpha}_+ \tan^{-1}\left(\frac{1}{2\bar{\alpha_+}}\right) - \bar{\alpha}_- \tan^{-1}\left(\frac{1}{2\bar{\alpha_-}}\right) + \frac{1}{4}\ln\left|\frac{4\bar{\alpha}_+^2+1}{4\bar{\alpha}_-^2+1}\right|\right]; \quad \text{(A.4)}$$

for $\bar{\alpha} < \delta\alpha$,

$$\Gamma_c^{-1} = -\frac{1}{2\delta\alpha}\left[\bar{\alpha}_+ \tan^{-1}\left(\frac{1}{\bar{\alpha_+}}\right) - \bar{\alpha}_- \tan^{-1}\left(\frac{1}{\bar{\alpha_-}}\right) + \frac{1}{2}\ln\left|\frac{\bar{\alpha}_+^2+1}{\bar{\alpha}_-^2+1}\right|\right]; \quad \text{(A.5)}$$

and for $|\bar{\alpha}| < -\delta\alpha$,

$$\Gamma_c^{-1} = I_1 + I_2, \quad \text{where} \quad \text{(A.6a)}$$

$$I_1 = \frac{\pi}{4}\left(\frac{\bar{\alpha_+}}{2\delta\alpha}\right) + \frac{1}{4\delta\alpha}\left[\bar{\alpha}_+ \tan^{-1}\left(\frac{1}{2\bar{\alpha_+}}\right) + \frac{1}{4}\ln\left|4\bar{\alpha}_+^2+1\right|\right], \quad \text{(A.6b)}$$

$$I_2 = -\frac{1}{2\delta\alpha}\left[-\bar{\alpha}_- \tan^{-1}\left(\frac{1}{\bar{\alpha_-}}\right) - \frac{1}{2}\ln\left|\bar{\alpha}_-^2+1\right|\right]. \quad \text{(A.6c)}$$

Similar to the results with a Lorentzian $g(\omega)$, it can be readily shown that Eqs. (A.4)-(A.5) reduce to Eqs. (A.2) and (A.3) in the limit $\delta\alpha \to 0$.

Next, we determine Γ_c when there is no spread in $h(\alpha)$, i.e., $h(\alpha) = \delta(\alpha - \bar{\alpha})$ where $\bar{\alpha}$ is constant, and the nonlinear frequency parameter $\bar{\gamma}$ is a nonzero constant for all oscillators. For $\bar{\alpha} < 0$, we know that $\bar{\gamma}$ does not affect stability of the state $\langle z \rangle = 0$, so Γ_c is still given by Eq. (A.3). For $\bar{\alpha} > 0$, we have, by substituting $s = i\Omega$ into the final expression after integration in Eq. (4.25), and introducing $\eta_\pm = \Omega \pm 1 + \bar{\alpha}\bar{\gamma}$, that Γ_c and Ω are to be given by the solution of the following pair of equations,

$$-4\Gamma_c^{-1} = \frac{\bar{\gamma}}{2}\ln\left|\frac{\eta_+^2(\eta_-^2+4\bar{\alpha}^2)}{\eta_-^2(\eta_+^2+4\bar{\alpha}^2)}\right| - \left[\pi + \tan^{-1}\left(\frac{\eta_+}{2\bar{\alpha}}\right) - \tan^{-1}\left(\frac{\eta_-}{2\bar{\alpha}}\right)\right], \quad \text{(A.7a)}$$

$$0 = \bar{\gamma}\left[\pi - \tan^{-1}\left(\frac{\eta_+}{2\bar{\alpha}}\right) + \tan^{-1}\left(\frac{\eta_-}{2\bar{\alpha}}\right)\right] + \frac{1}{2}\ln\left|\frac{\eta_+^2(\eta_+^2+4\bar{\alpha}^2)}{\eta_-^2(\eta_-^2+4\bar{\alpha}^2)}\right|. \quad \text{(A.7b)}$$

It can be easily checked from (A.7) that Γ_c reduces to (A.2) when $\bar{\gamma} \to 0$ (Note $\Omega \to 0$ in this limit).

Bibliography

[1] M. Abdulrehem and E. Ott, "Low dimensional description of pedestrian-induced oscillation of the Millennium Bridge," Chaos **19**, 013129 (2009).

[2] D. A. Abrams and S. H. Strogatz, "Chimera states in a ring of nonlocally coupled oscillators," Int. J. Bifur. Chaos **16**, 21 (2006).

[3] J. A. Acebron, L. L. Bonilla, C. J. P. Vincente, F. Ritort and R. Spigler, "The Kuramoto model: A simple paradigm for synchronization phenomena," Rev. Mod. Phys. **77**, 137 (2005).

[4] N. Akhmediev, J. M. Soto-Crespo and G. Town, "Pulsating solitons, chaotic solitons, period doubling, and pulse coexistence in mode-locked lasers: Complex Ginzburg-Landau equation approach," Phy. Rev. E **63**, 056602 (2001).

[5] T. M. Antonsen, R. T. Faghih, M. Girvan, E. Ott and J. Platig, "External periodic driving of large systems of globally coupled phase oscillators," Chaos **18**, 037112 (2008).

[6] I. S. Aranson and L. Kramer, "The world of the complex Ginzburg-Landau equation," Rev. Mod. Phys. **74**, 99 (2002).

[7] E. Barreto, B. Hunt, E. Ott and P. So, "Synchronization of networks of networks: The onset of coherent collective behavior in systems of interacting populations of heterogeneous oscillators," Phys. Rev. E **77**, 036107 (2008).

[8] J. Buck, "Synchronous Rhythmic Flashing of Fireflies, II," Q. Rev. Biol. **63**, 265 (1988).

[9] S. Chapman and T. G. Cowling, *The Mathematical Theory of Non-uniform Gases* (Cambridge University Press, 1952).

[10] M.Y. Choi, H.J. Kim, D. Kim and H. Hong, "Synchronization in a system of globally coupled oscillators with time delay," Phys. Rev. E **61**, 371 (2000).

[11] H. Daido and K. Nakanishi, "Aging Transition and Universal Scaling in Oscillator Networks," Phy. Rev. Lett. **93**, 104101 (2004).

[12] H. Daido and K. Nakanishi, "Diffusion-induced inhomogeneity in globally coupled oscillators: swing-by mechanism," Phy. Rev. Lett. **96**, 054101 (2006).

[13] S. Dano, F. Hynne, S. DeMonte, F. d'Ovidio, P. G. Sorensen and H. Westerhoff, "Synchronization of glycolytic oscillations in a yeast cell population," Faraday Discussions **120**, 261 (2002).

[14] R. J. Deissler and H. R. Brand, "Periodic, quasiperiodic, and chaotic localized solutions of the quintic complex Ginzburg-Landau equation," Phy. Rev. Lett. **72**, 478 (1994).

[15] B. Eckhardt, E. Ott, S. H. Strogatz, D. M. Abrams and A. McRobie, "Modeling walker synchronization on the Millennium Bridge," Phys. Rev. E **75**, 021110 (2007).

[16] G. B. Ermentrout, "Oscillator Death in Populations of "All To All" Coupled Nonlinear Oscillators,", Physica D **41**, 219 (1990).

[17] T. D. Frank, A. Daffertshofer, C. E. Peper, P. J. Beek and H. Haken, "Towards a comprehensive theory of brain activity: Coupled oscillator systems under external forces," Physica D **144**, 62 (2000).

[18] J. Garcia-Ojalvo, M. B. Elowitz and S. H. Strogatz, "Modeling a synthetic multicellular clock: Repressilators coupled by quorum sensing," Proc. Natl. Acad. Sci. **101**, 10955 (2004).

[19] L. Glass and M. C. Mackey, *From Clocks to Chaos: The Rhythms of Life* (Princeton University Press, NJ, 1988).

[20] V. Hakim and W.-J. Rappel, "Dynamics of the globally coupled complex Ginzburg-Landau equation," Phys. Rev. A, **46**, R7347 (1992).

[21] H. Hong, M. Y. Choi and B. J. Kim, "Synchronization on small-world networks," Phys. Rev. E **65**, 026139 (2002).

[22] T. Ichinomiya, "Frequency synchronization in a random oscillator network," Phys. Rev. E **70**, 026116 (2004).

[23] S. Kim, S. H. Park and C. S. Ryu, "Multistability in Coupled Oscillator Systems with Time Delay," Phys. Rev. Lett. **79**, 2911 (1997).

[24] I. Z.Kiss, Y. Zhai and J. L. Hudson, "Emergence Coherence in a Population of Chemical Oscillators," Sci. **296**, 1676 (2002).

[25] G. Kozyreff, A. G. Vladimirov and P. Mandel, "Global Coupling with Time Delay in an Array of Semiconductor Lasers," Phys. Rev. Lett. **85**, 3809 (2000).

[26] Y. Kuramoto, *International Symposium on Mathematical Problems in Theoretical Physics*, Lecture Notes in Physics, vol.39, edited by H. Araki (Springer-Verlag, Berlin, 1975).

[27] Y. Kuramoto, *Chemical Oscillations, Waves, and Turbulence* (Dover Press, Springer, 1984).

[28] Y. Kuramoto and D. Battogtokh, "Coexistence of Coherence and Incoherence in Nonlocally Coupled Phase Oscillators," Nonlinear Phenom. Complex Syst. **5**, 380 (2002).

[29] Y. Kuramoto, S. Shima, D. Battogtokh and Y. Shiogai, "Mean-Field Theory Revives in Self-Oscillatory Fields with Non-Local Coupling," Prog. Theor. Phys. Suppl. **161**, 127 (2006).

[30] C. R. Laing, "The dynamics of chimera states in heterogeneous Kuramoto networks," Physica D **238**, 1569 (2009).

[31] W. S. Lee, E. Ott and T. M. Antonsen, "Large Coupled Oscillator Systems with Heterogeneous Interaction Delays," Phys. Rev. Lett. **103**, 044101 (2009).

[32] W. S. Lee, E. Ott and T. M. Antonsen, "Phase and Amplitude Dynamics in Systems of Coupled Oscillators: Growth Heterogeneity, Nonlinear Frequency Shifts and Locked States," *in preparation.*

[33] W. S. Lee, E. Ott and T. M. Antonsen, "Phase and Amplitude Dynamics in Systems of Coupled Oscillators: Nonlinear Hetergeneities," *in preparation.*

[34] E. Martens, *et al.*, "Exact results for the Kuramoto model with a bimodal frequency distribution," Phys. Rev. E **79**, 026204 (2009).

[35] E. A. Martens, C. R. Laing and S. H. Strogatz, "Solvable Model of Spiral Wave Chimeras," Phys. Rev. Lett. **104**, 044101 (2010).

[36] S. A. Marvel and S. H. Strogatz, "Invariant submanifold for series arrays of Josephson junctions," Chaos **19**, 013132 (2009).

[37] P. C. Matthews, R. E. Mirollo and S. H. Strogatz, "Dynamics of a large system of coupled nonlinear oscillators," Physica D **52**, 293 (1991).

[38] P. C. Matthews, R. E. Mirollo and S. H. Strogatz, "Dynamics of a large system of coupled nonlinear oscillators," Physica D **52**, 293 (1991).

[39] D. C. Michaels, E. P. Matyas and J. Jalife, "Mechanisms of sinoatril pacemaker synchronization: a new hypothesis," Circulation Research **61**, 704 (1987).

[40] R. E. Mirollo and S. H. Strogatz, "Amplitude Death in an Array of Limit-Cycle Oscillators," J. Stat. Phys. **60**, 245 (1990).

[41] S. D. Monte, F. d'Ovidio, S. Danø and P. G. Sørensen, "Dynamical quorum sensing: Population density encoded in celluar dynamics," Proc. Natl. Acad. Sci. **104**, 18377 (2007).

[42] E. Montbrió, J. Kurths, and B. Blasius, "Synchronization of two interacting populations of oscillators," Phys. Rev. E **70**, 056125 (2004).

[43] E. Montbrió, D. Pazó and J. Schmidt, "Time delay in the Kuramoto model with bimodal frequency distribution", Phys. Rev. E **74**, 056201 (2006).

[44] E. Montbrió and D. Pazó, "Shear Diversity Prevents Collective Synchronization," Phys. Rev. Lett. **106**, 254101 (2011).

[45] Y. Moreno and A. F. Pacheco, "Synchronization of Kuramoto oscillators in scale-free networks," Europhys. Lett. **68**, 603 (2004).

[46] H. Mori and Y. Kuramoto, *Dissipative Structures and Chaos* (Springer 1998).

[47] N. Nakagawa and Y. Kuramoto, "From collective oscillations to collective chaos in a globally coupled oscillator system," Prog. Theor. Phys. **89** 313 (1993).

[48] N. Nakagawa and Y. Kuramoto, "From collective oscillations to collective chaos in a globally coupled oscillator system," Physica D **75**, 74 (1994).

[49] N. Nakagawa and Y. Kuramoto, "Anomalous Lyapunov spectrum in globally coupled oscillators," Physica D **80**, 307 (1995).

[50] S. Nichols and K. Wiesenfeld, "Ubiquitous neutral stability of splay-phase states," Phys. Rev. A **45**, 8430 (1992).

[51] O. E. Omel'chenko and M. Wolfrum, "Nonuniversal Transitions to Synchrony in the Sakaguchi-Kuramoto Model," Phys. Rev. Lett. **109** 164101 (2012).

[52] E. Ott, *Chaos in Dynamical Systems*, 2nd edition, Chapter 6, section 6.5 (Cambridge University Press, New York, 2002).

[53] E. Ott and T.M. Antonsen, "Low dimensional behavior of large systems of globally coupled oscillators," Chaos **18**, 037113 (2008).

[54] E. Ott and T.M. Antonsen, "Long time evolution of phase oscillator systems," Chaos **19** 023117 (2009).

[55] E. Ott, B. Hunt, and T.M. Antonsen, "Comment on "Long Time Evolution of Phase Oscillator Systems" [Chaos 19, 023117 (2009)]," Chaos **21** 025112 (2011).

[56] D. Pazó and E. Montbrió, "Universal behavior in populations composed of excitable and self-oscillatory elements," Phys. Rev. E, **73**, 055202 (2006).

[57] A. Pikovsky, M. Rosenblum and J.Kurths, *Synchronization: A Universal Concept in Nonlinear Sciences* (Cambridge University Press, 2004).

[58] J. G. Restrepo, E. Ott and B. R. Hunt, "Synchronization in large directed networks of coupled phase oscillators," Chaos, **16**, 015107 (2005).

[59] T. Roenneberg, *Internal Time: Chronotypes, Social Jet Lag, and Why You're So Tired* (Harvard University Press 2012).

[60] G. C. Sethia and A. Sen, "Clustered Chimera States in Delay-Coupled Oscillator Systems," Phys. Rev. Lett. **100** 144102 (2008).

[61] M. Shiino and M. Frankowicz, "Synchronization of infinitely many coupled limit-cycle type oscillators," Phys. Lett. A **136**, 103 (1989).

[62] S. Shima and Y. Kuramoto, "Rotating spiral waves with phase-randomized core in nonlocally coupled oscillators," Phys. Rev. E **69** 036213 (2004).

[63] S. Strogatz, *Sync: The Emerging Science of Spontaneous Order* (Hyperion 2003).

[64] S. H. Strogatz, "From Kuramoto to Crawford: exploring the onset of synchronization in populations of coupled oscillators," Physica D **143**, 1 (2000).

[65] S.H. Strogatz, D.M. Abrams, A.McRobie, B. Eckhardt and E.Ott, "Theoretical mechanics: Crowd synchrony on the Millennium Bridge," Nature **438**, 43 (2005).

[66] J. J. Suárez-Vargas, J. A. González, A. Stefanovska and P. V. McClintock, "Diverse routes to oscillator death in a coupled oscillator system," Europhys. Lett. **85**, 38008 (2009).

[67] A. F. Taylor, M. R. Tinsley, F. Wang, Z. Huang and K. Showalter, "Dynamical Quorum Sensing and Synchronization in Large Populations of Chemical Oscillators," Sci., **323**, 614 (2009).

[68] S. Yamaguchi, *et al.*, "Control Mechanism of the Circadian Clock for Timing of Cell Division in Vivo," Sci. **302**, 255 (2003).

[69] M.K. Stephen Yeung and S.H. Strogatz, "Time delay in the Kuramoto Model of Coupled Oscillators." Phys. Rev. Lett. **82**, 648 (1999).

[70] K. Wiesenfeld, C. Brawcikowski, G. James and R. Roy, "Observation of antiphase states in a multimode laser," Phys. Rev. Lett. **65**, 1749 (1990).

[71] A. T. Winfree, *The Geometry of Biological Time,* 2^{nd} *ed.* (Springer 2001).

[72] S. Yamaguchi, H. Isejima, T. Matsuo, R. Okura, K. Yagita, M. Kobayashi and H. Okamura, "Control Mechanism of the Circadian Clock for Timing of Cell Division in Vivo," Sci. **302**, 1408 (2003).

[73] J. Zamora-Munt, C. Masoller, J. Garcia-Ojalvo and R. Roy, "Crowd Synchrony and Quorum Sensing in Delay-Coupled Lasers," Phys. Rev. Lett. **105**, 264101 (2010).